Postischemic mild hypothermia alleviates hearing loss because of transient ischemia

Shoichiro Takeda[a], Nobuhiro Hakuba[c], Tadashi Yoshida[a], Kensuke Fujita[a], Naohito Hato[a], Ryuji Hata[b], Jun Hyodo[a] and Kiyofumi Gyo[a]

Departments of [a]Otolaryngology, [b]Functional Historogy, Ehime University School of Medicine, Shitsukawa, Toon, Ehime and [c]Department of Otolaryngology, Osaka Red Cross Hospital, Fudegasaki 5-30, Tennohji, Osaka, Japan

Correspondence to Dr Nobuhiro Hakuba, Department of Otolaryngology, Osaka Red Cross Hospital, Fudegasaki 5-30, Tennohji, Osaka 543-8555, Japan
Tel: +81 6 6774 5206; fax: +81 6 6774 5131; e-mail: hakubax@m.ehime-u.ac.jp

Received 7 May 2008; accepted 2 June 2008

DOI: 10.1097/WNR.0b013e32830b5f73

The effect of postischemic mild hypothermia on the inner ear has not been clarified. In this study, we investigated whether hypothermia after transient ischemia could prevent cochlear damage and its therapeutic time window. Mongolian gerbils were divided into six groups: a sham-operation group, a normothermia group, and four hypothermia groups in which hypothermia was induced 1–7, 1–4, 3–6, and 6–9 h after reperfusion. Animals subjected to postischemic mild hypothermia within 3 h after reperfusion had attenuated hearing loss and inner hair cell loss. The protective effect was greater when hypothermia was induced earlier and had a longer duration. This implies that mild hypothermia after ischemia could have therapeutic effects for inner ear ischemic damage. *NeuroReport* 19:1325–1328 © 2008 Wolters Kluwer Health | Lippincott Williams & Wilkins.

Keywords: cochlear ischemia, hair cell loss, hearing loss, mild hypothermia

Introduction

Hypothermia is thought to be an efficient procedure to alleviate ischemic damage of the brain. Deep hypothermia, however, causes complications such as lowering of blood flow, increased incidence of bacterial infection, and decreased cellular immunity [1–3]. In an experimental study with rats, Busto *et al.* (1989) demonstrated that ischemia-induced damages of the brain were prevented by the application of mild hypothermia [4]. Since then, many investigators studied the protective effects of mild hypothermia on the brain and reported similar results [5,6]. According to a recent clinical study, mild hypothermia increased the chance of recovery in comatose survivors of cardiac arrest [7]. These findings suggested that mild lowering of the body temperature might be sufficient to attenuate ischemic damage of neuronal tissue.

Over the last 10 years, we have studied the inner ear damage because of transient cochlear ischemia in gerbils. In our earlier study, we demonstrated that pre-ischemic mild hypothermia (32°C) was effective in preventing cochlear damage because of ischemia [8]. The effects of mild hypothermia applied after ischemia have, however, not been investigated. The purpose of this study was to determine if postischemic hypothermia could prevent cochlear damage, and if so, to reveal further the effective timing and duration of this procedure.

Materials and methods

The following experiments were conducted in accordance with the Guidelines for Animal Experimentation at Ehime University School of Medicine. Adult male Mongolian gerbils (*Meriones unguiculatus*) weighing 60–80 g were used. Anesthesia was induced with a mixture of 3% halothane and nitrous oxide/oxygen (7:3) gas and maintained with a mixture of 1% halothane gas. The animals were artificially ventilated using a small tube inserted through the mouth. The tidal volume was set to 1 ml and the rate to 70 times per minute. The Mongolian gerbil congenitally lacks the posterior cerebral communicating arteries and the cochlea receives their blood supply from the bilateral vertebral arteries by way of the basilar artery and the labyrinthine artery. Therefore, simultaneous occlusion of the bilateral vertebral arteries causes cochlear ischemia on both sides. The vertebral arteries were exposed bilaterally and dissected free from the surrounding connective tissues through a ventral midline incision of the neck [9]. Then, 4-0 silk ligatures were loosely looped around each artery. Cochlear ischemia was induced by pulling the ligatures with 5 g weights. After 15 min of ischemia, the sutures were removed to allow recirculation, which was confirmed by microscopic observation.

Hypothermia was introduced by placing the animal in a supine position on an ice bag. The temperature of the animal was monitored with a thermocouple probe (PTI-200, Unique Medical Corporation, Tokyo, Japan) inserted in the rectum. It was controlled by a thermo controller (TACT-2DF, Physitemp Corporation, New Jersey, USA) using a heating plate (HP-1M, Physitemp Corporation) and an ice bag. The rectal temperature was kept at 37 ± 1°C in normothermia, whereas it was kept at 32 ± 1°C in mild hypothermia. The

animals were divided into four groups on the basis of the timing of the start and end of hypothermia after reperfusion, 1–7 (n=6), 1–4 (n=14), 3–6 (n=8), and 6–9 h (n=8). As controls, some animals were subjected to sham operation (n=4) or normothermia after ischemia (n=16).

The hearing of animals was assessed before and 1, 4, and 7 days after ischemia. Under halothane anesthesia, auditory brain stem responses (ABRs) were recorded using a signal processor (NEC Synax 1200, NEC Medical Systems, Tokyo, Japan). The stimulus was introduced into the ear canal via a tiny polypropylene tube; thus each ear was stimulated separately. Recording needle electrodes were placed at the vertex and the retroauricle. In this study, we measured ABRs to 8000 Hz tone burst (0.5 ms rise/fall time and 10 ms duration), as hearing acuity at higher tones is more vulnerable to ischemic insult [10]. Responses to 300 consecutive stimuli were averaged, and the threshold of ABR was determined by measuring responses in 5 dB steps.

For histological study, animals were decapitated under deep anesthesia 7 days after ischemia. After the removal of the otic bullae, the cochleae were perfused with 4% paraformaldehyde in 0.1 M phosphate buffer at pH 7.4 into the scalae and postfixed for 2 h with the same fixative at 4°C. The specimens were immersed in phosphate-buffered saline (PBS) and the organ of Corti was dissected out by means of surface preparation technique under an operative microscope. The entire lateral and medial wall of the cochlear capsule was opened without disrupting the organ of Corti. Then, the basal turn of the organ of Corti was isolated and photographed with a camera (PM10SP, Olympus, Tokyo, Japan) through a microscope (BX60, Olympus). The specimen was then stained with rhodamine-phalloidin (Molecular Probes, Eugene, Oregon, USA) diluted 250 times in PBS containing 0.25% Triton X-100 and 1% bovine serum albumin for 30 min at room temperature. After rinsing in PBS, it was further stained with Hoechst 33342 (Calbiochem-Navabiochem Corporation, La Jolla, California, USA) dissolved in PBS, in a dark room for 1 h. It was again rinsed in PBS and mounted in carbonate-buffered glycerol (one part 0.5 M carbonate buffer at pH 9.5 to nine parts glycerol) containing 2.5% 1,4-diazabicyclo[2,2,2]octane to retard bleaching of the fluorescent signal. Fluorescence was detected using an Olympus BX60 microscope equipped with a green (BP 546, FT 580, LP 590 nm) and UV (BP 365, FT 395, LP 397 nm) filter. The number of intact and dead hair cells in the basal turn of the cochlea was quantified and the percentage of dead hair cells to whole hair cells was expressed. Earlier, we investigated the number of hair cells at each turn and the average number of inner hair cells (IHCs) at basal turn was about 300 in the gerbils [11]. In this study, we counted only the specimens that had at least 200 IHCs at the basal turn. We evaluated at least 200 of the IHCs at the basal turn.

Statistical differences of the data between each group were evaluated with Kruskal–Wallis test followed by Dunn's multiple comparison test. All values were represented as mean±SD. A P value of less than 0.05 was considered statistically significant.

Results

Sequential changes in ABR thresholds in the six groups are summarized in Fig. 1. In this figure, ABR threshold before the treatment was defined as 0 dB, and the subsequent increase of threshold is shown on the ordinate. In sham-operated controls, no substantial change in ABR was noted after the operation. In the normothermia group, the increase in the ABR threshold was 29.7±9.0 dB (mean±1 SD) on day 1 with a slight recovery on day 4, and recovered to 23.4±8.9 dB on day 7. In the hypothermia groups, the results depended on the timing and duration of hypothermia. When hypothermia was applied within 3 h after reperfusion, the increases in the ABR threshold were attenuated. The alleviating effects were more prominent when the postischemic cooling was initiated promptly and/or applied longer. The average increases in ABR threshold on day 7 in 1–7 h group, 1–4 h group, and 3–6 h group were 2.5±4.2, 7.9±13.4, and 15.6±10.2 dB, respectively. In contrast, a protective effect was not found in 6–9 h group; the average increase on day 7 was 23.8±4.4 dB, which was almost the same as in the normothermia group.

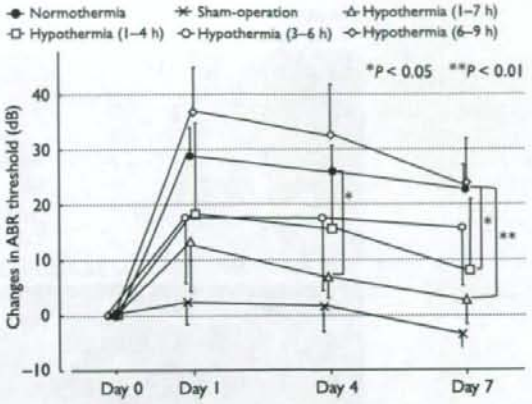

Fig. 1 Plots of brain stem response threshold over 7 days in the normothermic, sham-operated and hypothermic animals. Note that threshold elevations were greatest in the 6–9 h hypothermic animals, then normothermic animals, and lowest in the sham-operated controls. Intermediate thresholds were found in the animals exposed to hypothermia earlier in the procedure. The latter showed greater recovery than either normothermic or 6–9 h hypothermic animals. The data were represented by mean±1 SD.

Representative areas of the organ of Corti in each group on day 7 are shown in Fig. 2. Rhodamine-phalloidin staining permits the observation of the hair cell stereocilia, whereas Hoechst 33342 reveals the nuclei. In normothermia group, stereocilia and nuclei of the IHCs disappeared sporadically, as indicated by arrowheads. In contrast, such death of the IHCs was less in hypothermia groups. Sham-operated animals did not show substantial hair cell damage.

Ratios of dead IHCs on day 7 were compared among six groups. As shown in Fig. 3, the mean percentage of IHC loss was 16.3±3.5% in the normothermia group, whereas it was 0.3±0.4% in the sham-operated group. In hypothermia groups, damage of the hair cell was less than in the normothermia group, including the 6–9 h group. The percentages of dead IHCs in the 1–7 h group, 1–4 h group, 3–6 h group, and 6–9 h group were 5.1±2.7, 7.0±3.8, 10.1±4.7, and 13.4±5.6%, respectively. Statistically significant differences were noted between the 1–7 h group and the normothermia group (P<0.001), and between the 1–4 h group and the normothermia group (P<0.01). It should be noted that even 6–9 h of hypothermia was effective in reducing the number of dead IHCs. In all animals, loss of

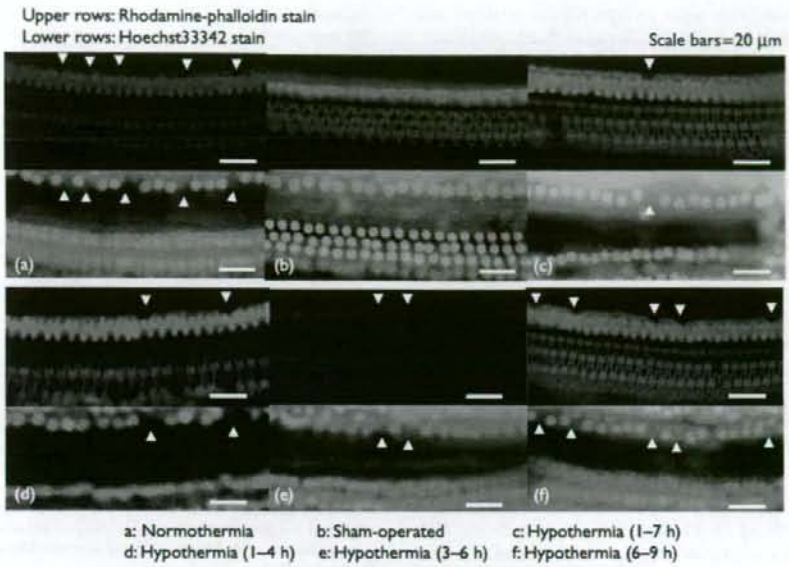

Fig. 2 Epifluorescence images of labeled organ of Corti from animals in each group 7 days after inducing ischemia or the sham operation. The specimen from the normothermia group shows that the stereocilia and nuclei of some inner hair cells (IHCs) had disappeared. In contrast, fewer dead cells were found in the groups subjected to hypothermia from 1 to 7, 1 to 4, and 3 to 6 h. However, the damage in the group that started hypothermia 6 h after reperfusion (i.e. 6–9 h) was similar to that in the normothermia group. Note the outer hair cells were remained almost intact. Scale bar=20 μm. Arrowheads indicate damaged IHCs.

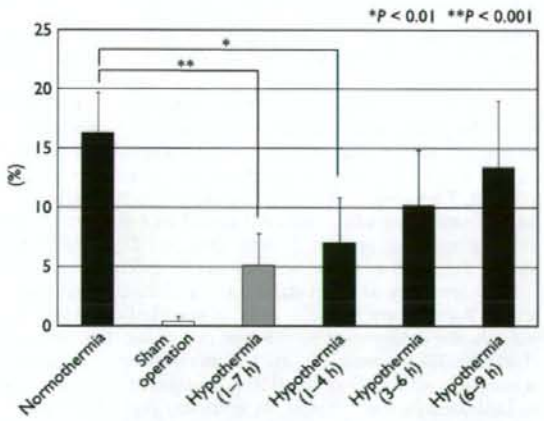

Fig. 3 The percentage of inner hair cells (IHCs) lost 7 days after surgery compared with the total number of IHCs at the basal turn in each group. These data indicated that the ratio of dead IHCs at the basal turn in hypothermic animals was fewer than that in normothermic animals. The protective effects were more prominent after earlier and/or longer application of hypothermia. It should be noted that even 6–9 h of hypothermia was effective in reducing the number of dead IHCs. The data were represented by mean ± 1 SD.

the outer hair cells was fewer than 3% on day 7 (data not shown). No statistical differences in the ratio of outer hair cell loss among the six groups were observed.

Discussion

In this study, postischemic mild hypothermia was effective in alleviating ischemic damage of the cochlea. At present, the protective mechanisms of hypothermia on inner ear tissue remain unclear.

Glutamate, an excitatory neurotransmitter in the cochlea, is thought to play an important role in the pathogenesis of ischemia-induced cochlear damage. In our studies of transient cochlear ischemia in the gerbil [12], we sequentially measured glutamate concentration in the perilymph after loading of ischemia and showed that glutamate levels abruptly increased immediately after ischemia but decreased rapidly thereafter. Watanabe *et al.* [8] demonstrated that hearing loss and the inner ear damage were completely prevented by pre-ischemic mild hypothermia. Hyodo *et al.* [13] considered that such protective effects were primarily through reduction of glutamate efflux, as the increase of glutamate concentration was completely prevented by pre-ischemic hypothermia. In this study, the postischemic hypothermia was started more than 1 h after ischemia when glutamate concentration was supposedly no longer high. This indicates that some mechanisms other than glutamate efflux may be involved in the protective effects of postischemic hypothermia. It may be that the protective mechanism of postischemic hypothermia is different from that of pre-ischemic hypothermia.

Inducible nitric oxide synthase (iNOS), which is generated by ischemic insult and produces excessive amounts of nitric oxide (NO), is considered responsible for delayed neuronal injury [14]. In the brain, the maximal enzymatic activity of iNOS has been noted to occur 1 day after ischemia [15]. Morizane *et al.* [16] showed that immunostaining for iNOS was positive in the organ of Corti and the spiral ganglion 1–4 days after transient ischemia. They further determined that NO concentration in the scala tympani was high on day 1, and returned to pre-ischemic level on day 7. Excessively produced NO leads to the formation of superoxide (O_2^-),

peroxynitrite ($ONOO^-$), and hydroxyl (OH^-) radicals [17], which are toxic especially to neuronal cells by working as oxidative stresses. According to recent in-vivo studies, hypothermia has been shown to inhibit all of these processes in the brain [18–21]. Thus, the cochlea might be protected by postischemic mild hypothermia through the attenuation of oxidative stress as in the brain.

As revealed in this study, postischemic mild hypothermia attenuated hearing impairment and hair cell loss when the body was cooled within 3 h after reperfusion. The protective effects were more prominent after earlier and/or longer application of hypothermia. Mild hypothermia of 6–9 h attenuated loss of IHCs, although it failed to prevent substantial increase in ABR threshold. The discrepancy between the ABR threshold and hair cell loss is probably because of the fact that the animals could not tolerate long-term experiments and produced weak ABR responses. The effects of postischemic mild hypothermia on the brain have also been studied in experimental cerebral infarction in rats. Ohta *et al.* reported that significant protective effects were observed when hypothermia was started within 4 h after reperfusion; they believe that treatment within 4 h is the therapeutic time window of postischemic mild hypothermia [22]. On the basis of these findings, we believe that mild hypothermia should be applied within 3–4 h after ischemic insult; later application of the procedure would not work well.

From a clinical point of view, mild hypothermia might be a promising option in the treatment of idiopathic sudden sensorineural hearing loss, as cochlear ischemia is considered one of the most possible causes of this disease [23–25]. Furthermore, hypothermia might also be applied in the treatment of other sensorineural hearing losses such as aminoglycoside ototoxicity, traumatic inner ear damage, noise-induced hearing loss, etc. This is because hypothermia has been shown to alter a variety of mechanisms, including metabolic enzymatic activity, inflammatory process, production of reactive oxygen species, and the expression/down-regulation of various genes [18]. Further study will be necessary to elucidate the effects of mild hypothermia on various types of inner ear damage because of causes other than ischemic insult.

Conclusion

Postischemic mild hypothermia is effective in attenuating hearing impairment and hair cell loss when the body was cooled within 3 h after reperfusion. The protective effects are more prominent by earlier and/or longer application of hypothermia. The present results suggested that mild hypothermia might be a promising procedure to attenuate inner ear damage because of idiopathic sudden sensorineural hearing loss that is supposed to be caused by cochlear ischemia.

Acknowledgements

The present study was supported in part by Grant-in-Aid for Young Scientists (B) (No. 20791199), Grant-in-Aid for Scientific Research (B) (No. 20390442), and Grant-in-Aid for Young Scientists (B) (No. 20791198), Ministry of Education, Science, Sports and Culture, Japan.

References

1. Hubert LR, Duncan AH. Cerebral blood flow and cerebral oxygen consumption during hypothermia. *Am J Physiol* 1954; **179**:85–88.
2. Andrea K, Daniel IS, Ralner L. Perioperative normothermia to reduce the incidence of surgical-wound infection and shorten hospitalization. *N Engl J Med* 1996; **334**:1209–1215.
3. Bebzion B, Yehuda S, Jacob R, Yaacov W, Alexander Z, Hanna B. Effects of mild perioperative hypothermia on cellular immune responses. *Anesthesiology* 1998; **89**:1133–1140.
4. Busto R, Globus MY-T, Dietrich WD, Martinez E, Valdes I, Ginsberg MD. Effect of mild hypothermia on ischemia-induced release of neurotransmitters and free fatty acids in rat brain. *Stroke* 1989; **20**:904–910.
5. Welsh FA, Sims RE, Harris VA. Mild hypothermia prevents ischemic injury in gerbil hippocampus. *J Cereb Blood Flow Metab* 1990; **10**:557–563.
6. Dietrich WD, Busto R, Alonso O, Globus MY-T, Ginsberg MD. Intraischemic but not postischemic brain hypothermia protects chronically following global forebrain ischemia in rats. *J Cereb Blood Flow Metab* 1993; **13**:541–549.
7. The Hypothermia After Cardiac Arrest Study Group. Mild therapeutic hypothermia to improve the neurologic outcome after cardiac arrest. *N Engl J Med* 2002; **346**:549–556.
8. Watanabe F, Koga K, Hakuba N, Gyo K. Hypothermia prevents hearing loss and progressive hair cell loss after transient cochlear ischemia in gerbils. *Neuroscience* 2001; **102**:639–645.
9. Hata R, Matsumoto M, Hatakeyama T, Ohtsuki T, Handa N, Niinobe M, *et al.* Differential vulnerability in the hindbrain neurons and local cerebral blood flow during bilateral vertebral occlusion in gerbils. *Neuroscience* 1993; **56**:423–439.
10. Hakuba N, Matsubara A, Hyodo J, Taniguchi M, Maetani T, Shimizu Y, *et al.* AMPA/kinate glutamate receptor antagonist reduces progressive inner hair cell loss after transient cochlear ischemia. *Brain Res* 2003; **25**:194–202.
11. Koga K, Hakuba N, Watanabe F, Shudou M, Gyo K. Transient cochlear ischemia causes delayed cell death in the organ of Corti: an experimental study in gerbils. *J Comp Neurol* 2003; **3**:105–111.
12. Hakuba N, Koga K, Shudou M, Watanabe F, Mitani A, Gyo K. Hearing loss and glutamate efflux in the perilymph following transient hindbrain ischemia in gerbils. *J Comp Neurol* 2000; **418**:217–226.
13. Hyodo J, Hakuba N, Koga K, Watanabe F, Shudou M, Taniguchi M, *et al.* Hypothermia reduces glutamate efflux in perilymph following transient cochlear ischemia. *Neuroreport* 2001; **12**:1983–1987.
14. Iadecola C, Zhang S, Casey R, Ross ME. Delayed reduction of ischemic brain injury and neurological deficits in mice lacking the inducible nitric oxide synthase gene. *J Neurosci* 1997; **17**:9157–9164.
15. Togashi H, Mori K, Ueno K, Matsumoto M, Suda N, Hideya S, *et al.* Consecutive evaluation of nitric oxide production after transient cerebral ischemia in the rat hippocampus using in vivo brain microdialysis. *Neurosci Lett* 1998; **240**:53–57.
16. Morizane I, Hakuba N, Hyodo J, Shimizu Y, Fujita K, Yoshida T, *et al.* Ischemic damage increases nitric oxide production via inducible nitric oxide synthase in the cochlea. *Nuerosci Lett* 2005; **391**:62–67.
17. Beckman JS, Beckman TW, Chen J, Marshall PA, Freeman BA. Apparent hydroxyl radical production by peroxynitrite: implications for endothelial injury from nitric oxide and superoxide. *Proc Natl Acad Sci U S A* 1990; **87**:1620–1624.
18. Liu L, Yenari MA. Therapeutic hypothermia: neuroprotective mechanisms. *Frontiers Biosci* 2007; **12**:816–825.
19. Maier CM, Ahern KvB, Cheng ML, Lee JE, Yenari MA, Steinberg GK, *et al.* Optimal depth and duration of mild hypothermia in a focal model of transient cerebral ischemia: effects on neurologic outcome, infarct size, apoptosis, and inflammation. *Stroke* 1998; **29**:2172–2180.
20. Phanithi PB, Yoshida Y, Santana A, Su M, Kawamura S, Yasui N. Mild hypothermia mitigates post-ischemic neuronal death following focal cerebral ischemia in rat brain: immunohistochemical study of Fas, caspase-3 and TUNEL. *Neuropath* 2000; **20**:273–282.
21. Baiping L, Xiujuan T, Hongwei C, Qiming X, Quling G. Effect of moderate hypothermia on lipid peroxidation in canine brain tissue after cardiac arrest and resuscitation. *Stroke* 1994; **25**:147–152.
22. Ohta H, Terao Y, Shintani Y, Kiyota Y. Therapeutic time window of post-ischemic mild hypothermia and the gene expression associated with the neuroprotection in rat focal cerebral ischemia. *Neurosci Res* 2007; **57**:424–433.
23. Smith GA, Gussen R. Inner ear pathologic features following mumps infection. *Arch Otolaryngol* 1976; **102**:108–110.
24. Cole RR, Jephrsdoerfer RA. Sudden hearing loss: an update. *Am J Otol* 1988; **9**:211–215.
25. Kim JS, Lopez I, DiPatre PL, Liu F, Ishiyama A, Baloh RW. Internal auditory artery infarction: clinicopathologic correction. *Neurology* 1999; **52**:40–44.

The FASEB Journal • Research Communication

Ramified microglial cells promote astrogliogenesis and maintenance of neural stem cells through activation of Stat3 function

Pengxiang Zhu,* Ryuji Hata,*,[1] Fang Cao,* Feng Gu,* Yasushi Hanakawa,† Koji Hashimoto,† and Masahiro Sakanaka*

*Department of Functional Histology and †Department of Dermatology, Ehime University Graduate School of Medicine, Shitsukawa, Toon, Ehime, Japan

ABSTRACT **The differentiation and proliferation of neural stem cells (NSCs) are regulated by a combination of their intrinsic properties (*e.g.*, transcription factors, epigenetic factors, and microRNA regulation) and cell-extrinsic properties from the microenvironment around NSC (*e.g.*, cytokines, growth factors, and cell-cell contact). Recently, there has been a great interest in clarifying the mechanism of the influence of the microenvironment on NSCs, especially cell-cell contact between NSCs and other types of cells nearby. In this study, we investigated whether microglial (Mi) cells influence the fate of NSCs. Coculture study showed that ramified Mi cells promoted astrogliogenesis and maintenance of NSCs through their paracrine effects. This microglia-induced astrogliogenesis was inhibited by AG490 and by overexpression of the dominant-negative form of Stat3 and SOCS3. Promoter assay revealed transactivation of Stat3 function in NSCs by Mi cells. Gene expression study revealed that mRNA of Notch family members (notch1–3) and sox9 in NSCs was significantly upregulated by Mi cells, and this up-regulation was inhibited by AG490. These results demonstrated that ramified Mi cells promoted astrogliogenesis and maintenance of NSCs by activating Stat3 function and *via* notch and sox9 signaling pathways.—Zhu, P., Hata, R., Cao, F., Gu, F., Hanakawa, Y., Hashimoto, K., Sakanaka, M. Ramified microglial cells promote astrogliogenesis and maintenance of neural stem cells through activation of Stat3 function. *FASEB J.* 22, 3866–3877 (2008)**

Key Words: neurogenesis · NSC · SOCS3 · AG490 · notch

DURING BRAIN DEVELOPMENT, neural stem cells (NSCs) are produced within germinal zones in close contact with the lateral ventricle walls. The self-renewal, proliferation, and differentiation of NSCs are regulated by the combination of their intrinsic properties (*e.g.*, transcription factors, epigenetic factors, and microRNA regulation) and cell-extrinsic properties from the microenvironment around NSCs: the stem cell niche (*e.g.*, cytokines, growth factors and cell-cell contact; ref. 1). It is reasonable to believe that the interactions between precursor cells and the microenvironment faced by cells influence their differentiation. In accordance with this hypothesis, astrocytes influence the neuronal fate commitment of adult hippocampal NSCs (2), suggesting the importance of cell-cell interactions between glial cells and NSCs. In addition, recent studies (3, 4) have demonstrated that microglial cells play an important role in neurogenesis.

Microglial cells are hematopoietic in origin and have functions similar to those of other tissue macrophages, including phagocytosis, antigen presentation, and production of cytokines, chemokines, eicosanoids, complement components, matrix metalloproteinases, oxidative radicals, and nitric oxide (NO; ref. 5). In the normal brain, microglial cells display a quiescent phenotype. On insult to the brain, microglial cells became highly activated and express the products mentioned above. Activation of microglial cells can result in either neuroprotective or neurotoxic effects, or both. Even in the quiescent form, microglial cells can express and secrete several neurotrophic factors, as well as several cytokines and chemokines (6).

Because microglial cells have been implicated in a variety of mechanisms of neuronal development and function (7), we investigated the effects of ramified microglial cells that secreted neither interleukin (IL) -6 nor NO on the fate of NSCs. Here, we demonstrated that ramified microglial cells promoted astrogliogenesis and maintenance of NSCs through activation of Stat3 function.

MATERIALS AND METHODS

All experiments were approved by the Ethics Committee of Ehime University Graduate School of Medicine and were conducted according to the Guidelines for Animal Experimentation at Ehime University Graduate School of Medicine.

[1] Correspondence: Department of Functional Histology, Ehime University Graduate School of Medicine, Shitsukawa, Toon, Ehime 791-0295, Japan. E-mail: hata@m.ehime-u.ac.jp

doi: 10.1096/fj.08-105908

0892-6638/08/0022-3866 © FASEB

Neurosphere generation and maintenance

NSCs were isolated from E-17 rats (Wistar rats; Charles River Laboratories, Inc., Yokohama, Japan). The meninges of embryonic rat brains were carefully cleared. The striatal tissue was separated from both hemispheres with fine forceps and was mechanically triturated. Cells were seeded in 9-cm dishes (Sumilon MS13900; Sumitoko Bakelite, Tokyo, Japan) in growth medium composed of Dulbecco modified Eagle medium (DMEM; Sigma Chemical, St. Louis, MO, USA) containing 0.2 mg/ml bovine serum albumin (A-7638, Sigma Chemical), 10 mM HEPES, 4.5 mg/ml glucose, 5 μg/ml insulin, 5 nM sodium selenite, 5 μg/ml transferrin, and 40 ng/ml human recombinant epidermal growth factor (Upstate Biotechnology, Lake Placid, NY, USA). Antibiotics and antimycotics (100 U/ml penicillin and 0.25 μg/ml amphotericin B) were also included. NSCs were grown as neurospheres.

Microglial cell culture

The forebrains of newborn Wistar rats were dissected out, and cell suspensions were obtained by passing the tissues through a nylon mesh (160 μm). The suspended cells were seeded in poly-L-lysine (mean M_r 40,750; Sigma Chemical) -coated 80 cm^2 culture flasks (BD Biosciences, San Jose, CA, USA). They were cultured at 37°C in 5% CO_2 and nearly 100% humidity in DMEM supplemented with 10% fetal calf serum. The culture medium was changed every 2 days. Twelve to 14 days later, microglial cells were isolated according to the method of Suzumura *et al.* (8) with modification. In brief, microglial cells were detached from the astrocyte monolayers in the culture flasks by mechanical shaking and reseeded on 10-cm polystyrene dishes (Suspension Culture Dish; Corning, Corning, NY, USA). The cells were incubated for 10 min at 37°C, and then the dishes were washed twice with serum-free DMEM. The cells attached to the dishes were collected with a scraper and suspended in neurosphere-differentiating medium (Neurobasal medium: Invitrogen, Gaithersburg, MD, USA) containing B27 supplement (Invitrogen), all-trans-retinoic acid (1.0×10^{-7} M), 2 mM L-glutamine, and antibiotics (50 U/ml penicillin and 50 μg/ml streptomycin). Some of the microglial cells were seeded onto 9-cm dishes (Sumilon MS13900, Sumitoko Bakelite) at a density of 1.4×10^5/ml or 4.0×10^5/ml and incubated in the same differentiating medium. Twenty-four hours later, the medium was collected, centrifuged for 15 min at 1500 rpm to remove debris, and used as microglia-conditioned medium (MCM).

Coculture of microglial cells with NSCs

Five days after seeding of triturated cells from the striatal tissue, they were dissociated mechanically and reseeded into poly-L-lysine-coated 24-well plates at a density of 5.0×10^5/well in neurosphere-differentiating medium (Neurobasal medium; Invitrogen) containing B27 supplement (Invitrogen), all-trans-retinoic acid (1.0×10^{-7} M), 2 mM L-glutamine, and antibiotics (50 U/ml penicillin and 50 μg/ml streptomycin). Four hours later, after we confirmed that NSCs had attached to the bottom of the wells, three types of coculture of NSCs with microglial cells were prepared as follows:

Mixed type

Microglial cells (0, 0.7×10^5, or 2.0×10^5/well) were added directly to NSC cultures in a 24-well plate.

Insert type

Microglial cells (0, 0.7×10^5, or 2.0×10^5/well) were seeded into cell culture inserts (0.4 μm pore size, BD Bioscience) that were placed on the top of a 24-well plate containing NSCs.

Conditioned type

Medium in a 24-well plate containing NSCs was changed to MCM (conditioned medium from 24 h microglia cultures based on neurosphere-differentiating medium at a density of 1.4×10^5/ml or 4.0×10^5/ml). The neurosphere-differentiating medium was changed every 2 days, and MCM was changed every day.

Adenoviral vectors

A recombinant adenovirus expressing human SOCS3 was constructed as described previously (9). Human SOCS3 DNA was excised, and the resultant expression units were inserted at the SwaI site of the cosmid vector pAxCAwt (RBD:1678; Bio Resource Center, Riken, Wako, Japan). To make a dominant-negative form of murine Stat3 (Stat3F), the tyrosine residue at 705 of Stat3 was replaced with phenylalanine (Y705F; ref. 10). Stat3F DNA was excised, and the resultant expression units were inserted at the SwaI site of pAxCAwt. To generate recombinant adenoviruses (Ad.SOCS3 and Ad.Stat3F), cosmid DNA was cotransfected with the DNA-terminal protein complex into human kidney 293 cells. A recombinant adenovirus expressing β-galactosidase (Ad.Lz) was provided by Dr. Izumu Saito (University of Tokyo, Tokyo, Japan). Each recombinant virus was propagated in 293 cells and purified by CsCl step-gradient ultracentrifugation. Viral titers were determined using the modified end point cytopathic effect assay (11).

Application of inhibitors or adenoviral vectors

After growth medium was changed to neurosphere-differentiating medium or MCM, inhibitors or adenoviral vectors were applied to NSCs. The inhibitors used were as follows: LY294002 (CAS 154447-36-6; Promega, Madison, WI, USA) at 10 μm/ml, Noggin (R&D Systems, Minneapolis, MN, USA) at 20 ng/ml, PTP inhibitor II (cat. 540205, CAS 2632-13-5; Calbiochem, La Jolla, CA, USA) at 0.1 nm/ml, and AG490 (cat. 658401; Calbiochem) at 1 μm/ml. Our preliminary experiments revealed that inhibitors had no cytotoxic effects on NSCs at the concentrations used in this study, whereas they showed some cytotoxic effects on NSCs at 10× higher concentrations (data not shown). Adenoviral vectors expressing SOCS3, Stat3F, or Lz [multiplicity of infection (MOI) =10] were also applied to NSCs. For quantitative real-time polymerase chain reaction (PCR) and Western blot analysis, cells were collected at 1 or 3 days after the application of inhibitors or adenoviral vectors.

Immunoblot analysis

Cells were solubilized in Laemmli's lysis buffer containing 2% sodium dodecyl sulfate (12). The suspension was resolved by electrophoresis, transferred to nitrocellulose sheets, and immunoblotted using a rabbit polyclonal antibody against glial fibrillary acidic protein (GFAP; G9269; Sigma) or mouse monoclonal antibodies against β-actin (A5441; Sigma), Stat3 (sc-8019; Santa Cruz Biotechnology, Santa Cruz, CA, USA), pStat3 (Tyr705-phosphorylated Stat3; sc-8059; Santa Cruz Biotechnology), SOCS3 (sc-9023; Santa Cruz Biotechnology), microtubule-associated protein 2 (MAP2; Sternberger Monoclonals, Lutherville, MD, USA), Tuj1 (MMS-435P; Covance Research, Berkeley, CA, USA), and Nestin (MAB353; Chemicon, Temecula, CA, USA) proteins. The second antibodies were alkaline phosphatase-conjugated anti-rabbit immunoglobulin G (IgG) for the rabbit polyclonal antibody or alkaline phosphatase-conjugated anti-mouse IgG for the mouse monoclonal antibodies. The density of immunoreac-

tive bands was measured using NIH image software (National Institutes of Health, Bethesda, MD, USA).

Luciferase promoter assay

The constructs of the Stat3 reporter plasmids have been described elsewhere (9). In brief, the Stat3F reporter plasmid contained 4 copies of the acute-phase response element (APRE) in front of the minimal junB promoter linked to the luciferase gene. The response element was the APRE of the rat α2-macroglobulin gene (5′-GCGCCTTCTGGGAAGATC-CTTACGGGAATTCAG-3′). The cultured neurospheres were washed once in PBS, triturated, and resuspended in the specified electroporation buffer to a final concentration of 1.0×10^7 cells/ml. Then, 10 μg Stat3 reporter plasmid and 4 μg pRL-TK (Promega) internal control plasmid DNA were mixed with 0.1 ml cell suspension, transferred to a 2.0-mm electroporation cuvette, and electroporated with an Amaxa Nucleofector apparatus (Amaxa, Cologne, Germany). Then transfected neurospheres were exposed to adenoviral vectors expressing SOC3, Stat3F, or Lz (MOI=10) for 1 h in differentiating medium or MCM. Some transfected neurospheres were treated with both mouse leukemia inhibitory factor (LIF; 30 ng/ml; Chemicon, Temecula, CA, USA) and human basic fibroblast growth factor (bFGF; 10 ng/ml; Genzyme Techne, Minneapolis, MN, USA) or both rat IL-6 (30 ng/ml; Peprotech, London, UK) and human sIL-6R (30 ng/ml, Peprotech) as a positive control. Two days after electroporation, the activity of firefly luciferase from the Stat3 promoter-luciferase plasmid and renilla luciferase from the pRL-TK plasmid in the cell extracts was evaluated using a dual-luciferase assay kit (Promega) with a luminometer (TD-20/20; Turner Designs, Sunnyvale, CA, USA). Relative firefly luciferase activity was calculated by normalizing the transfection efficiency according to the renilla luciferase activity.

Quantitative real-time PCR

Cells were washed with PBS, and total RNA was extracted using Isogen (Nippon Gene, Tokyo, Japan). Total RNA was digested with DNase, and then single-stranded cDNA was obtained using oligo dT primers and Moloney murine leukemia virus reverse transcriptase (Life Technologies, Rockville, MD, USA). For quantitative real-time PCR, TaqMan real-time PCR analysis was carried out. The oligonucleotide primers and TaqMan fluorogenic probe for each gene were purchased commercially (Applied Biosystems, Foster City, CA, USA; **Table 1**). Reactions were run on an ABI Prism 7700 sequence detection system (Applied Biosystems). The cycling conditions were 10 min polymerase activation at 95°C followed by 40 cycles at 95°C for 15 s and 60°C for 60 s. β-Actin was used as the internal control. Threshold cycle (Ct) values of the target genes were normalized to those of the internal control genes. The relative expression in each sample to that of the control sample was calculated according to the $2-\Delta\Delta CT$ method (13).

Immunocytochemistry

Cells were washed with PBS and fixed for 30 min with 4% paraformaldehyde in 0.1 M phosphate buffer (pH 7.4). After 3 washes with PBS, the samples were incubated with 10% normal goat serum dissolved in PBS. Either a primary mouse monoclonal antibody against MAP2 (Sternberger Monoclonals) or a rabbit polyclonal antibody against GFAP (Sigma) was incubated with the samples at 4°C overnight. The samples were washed 3 times with PBS, incubated with rhodamine-conjugated goat anti-mouse IgG (ICN, Irvine, CA, USA) or with fluorescein-5-isothiocyanate-conjugated goat anti-rabbit IgG (ICN) for 30 min at room temperature, washed 3 times with PBS and mounted in Vectashield (Vector Lab, Burlingame, CA, USA). The cells were counterstained with Hoechst 33342 (B2261; Sigma) to identify nuclei.

Enzyme-linked immunosorbent assay (ELISA) and NO assay

Microglial cells at a density of 4.0×10^5/ml were cultured for 24 h in neurosphere-differentiating medium. After their settlement was confirmed, cells were cultured with fresh neurosphere-differentiating media in the presence and absence of lipopolysaccharide (LPS; 1 μg/ml). One day later, the supernatants were collected and the assays were per-

TABLE 1. *Assay identifiers and gene names*

Assay ID	Gene name
Rn00667869_m1	β-actin
Rn00561420_m1	Interleukin 6
Rn00573491_g1	Leukemia inhibitory factor (LIF)
Rn00755092_m1	Ciliary neurotrophic factor (CNTF)
Rn00567503_m1	Cardiotrophin 1 (CT1)
Rn00567818_m1	Bone morphogenetic protein 2 (BMP2)
Rn00563202_m1	Bone morphogenetic protein 4 (BMP4)
Rn00570809_m1	Fibroblast growth factor 2 (FGF2)
Rn00563336_m1	Epidermal growth factor (EGF)
Rn01758634_g1	Notch 1
Rn00577522_m1	Notch 2
Rn00571731_m1	Notch 3
Rn00577566_m1	Hairy and enhancer of split 1 (Hes1)
Rn00821207_g1	Hairy and enhancer of split 5 (Hes5)
Rn00562985_s1	Inhibitor of DNA binding 1 (Id1)
Rn00564939_g1	Inhibitor of DNA binding 2 (Id2)
Rn00564927_m1	Inhibitor of DNA binding 3 (Id3)
Rn00574345_m1	Achaete-scute complex homolog-like 1 (Mash1)
Rn00824571_s1	Neurogenic differentiation 1 (NeuroD1)
Rn02132577_s1	Neurogenic differentiation 2 (NeuroD2)
Rn01751069_mH	SRY-box containing gene 9 (Sox9)

formed. The concentrations of IL-1β, IL-6, and tumor necrosis factor (TNF) -α in the supernatants were measured by ELISA. The nitrite levels were determined after mixing equal amounts of supernatant and Griess reagent [*N*-(1-naphthyl)-ethylenediamine (0.1%) and sulfanilamide (1%)] (Sigma). ELISA kits were purchased from BioSource USA (Camarillo, CA, USA) and used according to the manufacturer's protocol. Sodium nitrite (Sigma) was used as a standard solution.

Statistical analysis

All values are presented as means ± SD. The levels of nitrite and cytokines in the presence and absence of LPS were analyzed statistically by unpaired *t* test. All the other statistical significances were tested by one-way ANOVA followed by Bonferroni's multiple comparison test. A value of $P < 0.05$ was considered statistically significant.

RESULTS

Coculture with microglial cells promotes astrogliagenesis in NSCs

We first examined whether coculture of NSCs with microglial cells could modulate the differentiation of NSCs. To address this issue, microglial cells (0, 0.7×10^5, or 2.0×10^5/well) were directly added to NSC culture (5.0×10^5/well) in 24-well plates (mixed type). At 3 days after coculture, cells were homogenized in lysis buffer and immunoblotted with an antibody against GFAP (a specific marker of astrocytes) or MAP2 (a specific marker of neurons). Experiments were carried out 5 times independently. Densitometric analysis revealed that 3 days after coculture, the level of GFAP protein in NSCs with microglial cells (0.7×10^5 and 2.0×10^5/well) was significantly increased (~1.7- and 1.7-fold, respectively) compared with that in the control without microglial cells, whereas the level of MAP2 protein did not differ among the three groups (**Fig. 1*A–C***).

To prevent physical interactions between NSCs and microglial cells, we performed another type of coculture in which the two cell populations were cultured in the same well, but were separated by a culture insert membrane that permitted medium exchange without physical contact between NSCs and microglial cells (insert type). Microglial cells (0, 0.7×10^5, or 2.0×10^5/well) were seeded into cell culture inserts that were placed on the top of a 24-well plate containing neurospheres. Three days after coculture, the level of GFAP protein in neurospheres with microglial cells was significantly increased (~2.0- and 2.2-fold) compared with that in the control without microglial cells, whereas the level of MAP2 protein did not differ among the three groups (Fig. 1*D–F*).

Because coculture study using culture inserts suggested that the effect of microglial cells on NSC differentiation was related to diffusible factors released by microglial cells in the medium, we next investigated the effects of MCM on the fate of NSCs. Medium in a 24-well plate containing neurospheres was changed to the conditioned medium from 24 h microglia cultures at a density of 0, 1.4×10^5/ml, or 4.0×10^5/ml (conditioned type). Three days after culture with MCM, the level of GFAP protein in NSCs cultured with MCM (1.4×10^5/ml and 4.0×10^5/ml) was significantly increased (~1.8- and 1.7-fold) compared with that in the control without MCM, whereas the level of MAP2 protein did not differ among the three groups (Fig. 1*G–I*).

Taken together, these results showed that microglial cells promoted astrogliogenesis in NSCs and that this microglia-induced astrogliogenesis was not related to physical contact between the two cell populations but to some diffusible factors released by microglial cells. Hence, thereafter, we investigated the mechanisms of microglia-induced astrogliogenesis by using MCM (conditioned type).

AG490 inhibits microglia-induced astrogliogenesis in NSCs, whereas LY29002, PTPII, and Noggin do not

To clarify the mechanism of microglia-induced astrogliogenesis in NSCs, we applied reagents to inhibit the cell signaling for modulating the fate of NSCs. After NSCs were seeded into 24-well plates at a density of 5.0×10^5/well, they were incubated with MCM (conditioned medium from 24 h microglia cultures at a density of 1.4×10^5/ml) in the presence and absence of these inhibitors. One or 3 days later, the cells were homogenized in lysis buffer and immunoblotted with antibodies against GFAP or MAP2. Experiments were carried out 5 times independently. Densitometric analysis revealed that a phosphoinositide 3-kinase (PI3K) inhibitor (10 μm/ml LY294002) did not inhibit microglia-induced astrogliogenesis (**Fig. 2**). Furthermore, a BMP-specific antagonist (20 ng/ml Noggin) and an SHP (Src homology 2 domain-containing tyrosine phosphatase) inhibitor (0.1 nm/ml PTP inhibitor II) did not inhibit this astrogliogenesis (**Figs. 3** and **4**). However, a Jak2 kinase inhibitor (1 μm/ml AG490) inhibited microglia-induced astrogliogenesis in NSCs (**Fig. 5**). Three days after incubation, the level of GFAP protein in NSCs with MCM was significantly increased (1.8-fold) compared with that in NSCs without MCM. With the addition of AG490, the level of GFAP protein was reduced to the control level (Fig. 5*F*). These results showed that the Jak/Stat signaling pathway played a crucial role in astrogliogenesis of NSCs mediated by microglial cells.

To confirm whether the increase of GFAP is really due to the increase of the number of astrocytes, we performed immunostaining for counting cell numbers. After NSCs were seeded into 24-well plates at a density of 2.0×10^5/well, they were incubated with neurosphere-differentiating medium or MCM in the presence or absence of AG490 (1 μm/ml). Three days later, expression of differentiation markers was evaluated by immunostaining with antibodies against GFAP and MAP2. Cells that were positive for MAP2 or GFAP were scored in 10 to 15 random nonoverlapping fields (400 μm^2) in each experiment. The proportion of MAP2

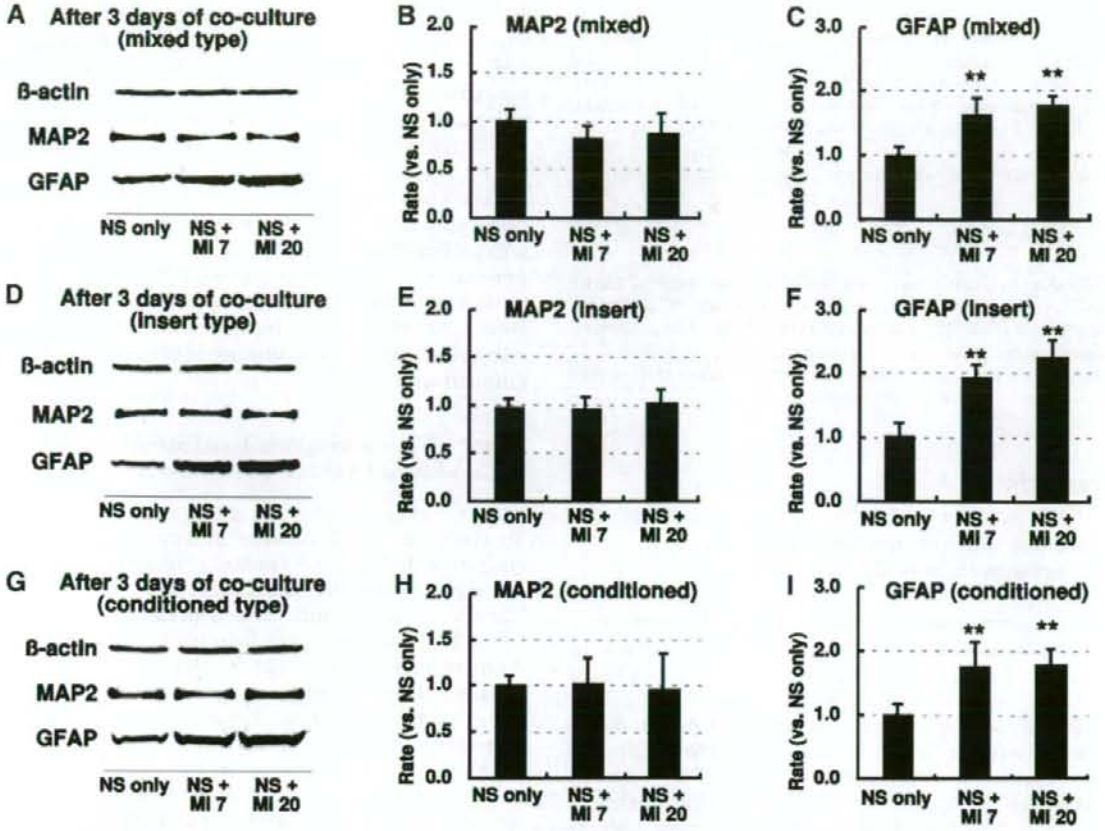

Figure 1. Effects of microglial (MI) cells on the fate of NSCs (NS) after 3 days of coculture. Microglial cells (0, 0.7×10^5, or 2.0×10^5/well) were directly added to NSC cultures (5.0×10^5/well) in 24-well plates (mixed type; *A–C*) or seeded into cell culture inserts that were placed on the top of a 24-well plate containing NSCs (insert type; *D–F*); or medium in a 24-well plate containing NSCs was changed to conditioned medium from 24 h microglia cultures at a density of 0, 1.4×10^5/ml, or 4.0×10^5/ml (conditioned type; *G–I*). At 3 days after coculture, cells were homogenized in lysis buffer and immunoblotted with an antibody against GFAP or MAP2. Experiments were carried out 5 times independently. Note that the protein level of GFAP was significantly increased in all three types of coculture. $^{**}P < 0.01$ *vs.* NS only.

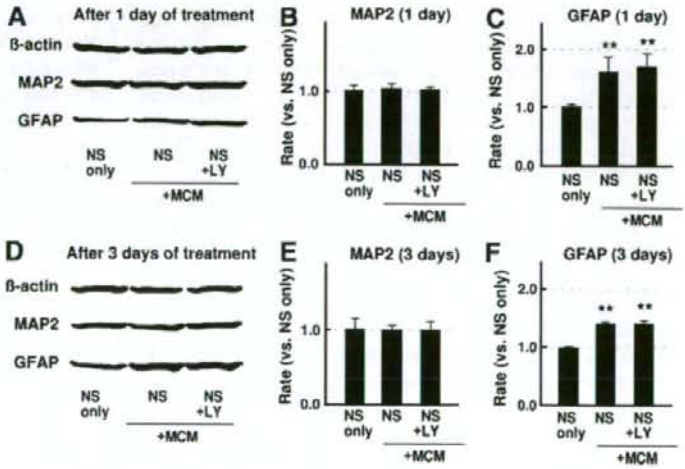

Figure 2. Effects of LY294002 (LY) on NSCs cultured in MCM. After NSCs were seeded into 24-well plates at a density of 5.0×10^5/well, NSCs were incubated with MCM in the presence and absence of LY294002 (10 μm/ml; a PI3K inhibitor). One day (*A–C*) or 3 days later (*D–F*), cells were homogenized in lysis buffer and immunoblotted with antibodies against GFAP or MAP2. Experiments were carried out 5 times independently. Note that the protein levels of GFAP and MAP2 did differ irrespective of the presence of LY294002. $^{**}P < 0.01$ *vs.* NS only.

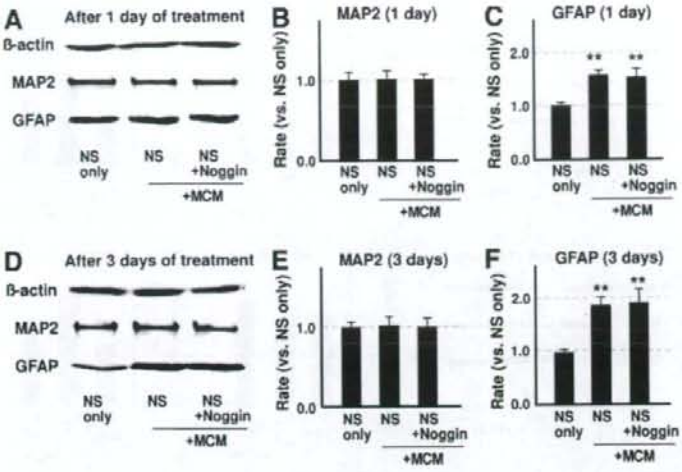

Figure 3. Effects of Noggin on NSCs cultured in MCM. After NSCs were seeded into 24-well plates at a density of 5.0×10^5/well, NSCs were incubated with MCM in the presence and absence of Noggin (20 ng/ml; a BMP-specific antagonist). One day (*A–C*) or 3 days later (*D–F*), cells were homogenized in lysis buffer and immunoblotted with antibodies against GFAP or MAP2. Experiments were carried out 5 times independently. Note that the protein levels of GFAP and MAP2 were not different irrespective of the presence of Noggin. $^{**}P < 0.01$ *vs.* NS only.

and GFAP positive cells was expressed as a percentage of the MAP2 and GFAP positive cells to Hoechst 33342 positive cells, respectively. As shown in **Fig. 6**, MCM significantly increased the proportion of the GFAP-positive cells and this increase was inhibited by the treatment of AG490 [15.1±0.5% of total cells in neurosphere-differentiating medium, 34.2±0.6% in MCM, and 15.9±0.6% in MCM with AG490]. These data also suggested that MCM promoted astrogliogenesis of NSCs and that this MCM-induced astrogliogenesis was inhibited by AG490.

Stat3F and SOCS3 inhibit microglia-induced astrogliogenesis in NSCs

It is well known that Stat3 plays crucial roles in determining the fate of NSCs. Enhancement of Stat3 activity in NSCs leads to subsequent glial differentiation (14). Our inhibitor study showed that AG490, a Jak2 kinase inhibitor, suppressed microglia-induced astrogliogenesis, suggesting that the Jak/Stat signaling pathway, especially activation of Stat3 function, played a crucial role in microglia-induced astrogliogenesis in NSCs. To confirm this assumption, we used two types of adenovirus vectors expressing Stat3F and SOCS3. Stat3F is a dominant-negative form of Stat3. In this mutant (Stat3F), the tyrosine residue at amino acid position 705 of murine Stat3 is mutated to phenylalanine. Stat3F binds to the gp130 receptor, which in turn leads to competitive inhibition of phosphorylation of endogenous Stat3 on activation of the gp130 receptor. When expressed at high levels, Stat3F has been shown to block activation of endogenous Stat3 in various types of cells including NSCs (10). SOCS3 has been shown to interact with gp130 and Jak, and this interaction results in relatively specific inhibition of gp130 signaling (15). Moreover, SOCS3 has been shown to block activation of endogenous Stat3 in NSCs (9).

By using these two types of adenovirus vectors, we examined whether microglia-induced astrogliogenesis was inhibited by blocking the activation of endogenous Stat3 in NSCs. After NSCs were seeded into 24-well plates at a density of 5.0×10^5/well, they were inoculated with an adenovirus vector expressing Stat3F,

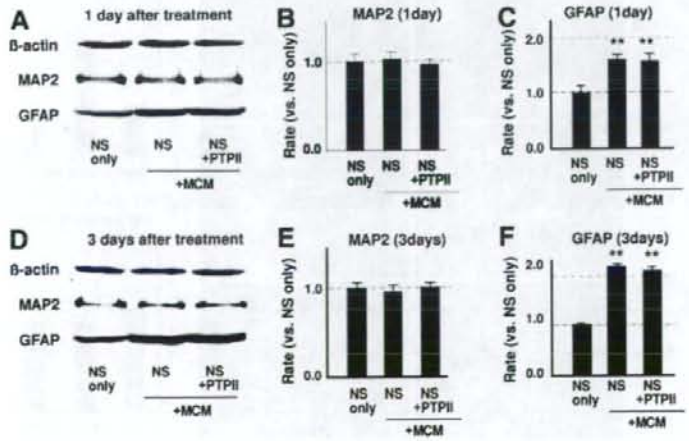

Figure 4. Effects of PTP inhibitor II on NSCs cultured in MCM. After NSCs were seeded into 24-well plates at a density of 5.0×10^5/well, NSCs were incubated with MCM in the presence and absence of a PTP inhibitor II (0.1 nm/ml PTPII; an SHP inhibitor). One day (*A–C*) or 3 days later (*D–F*), the cells were homogenized in lysis buffer and immunoblotted with antibodies against GFAP or MAP2. Experiments were carried out 5 times independently. Note that the protein levels of GFAP and MAP2 did not differ irrespective of the presence of PTP inhibitor II. $^{**}P < 0.01$ *vs.* NS only.

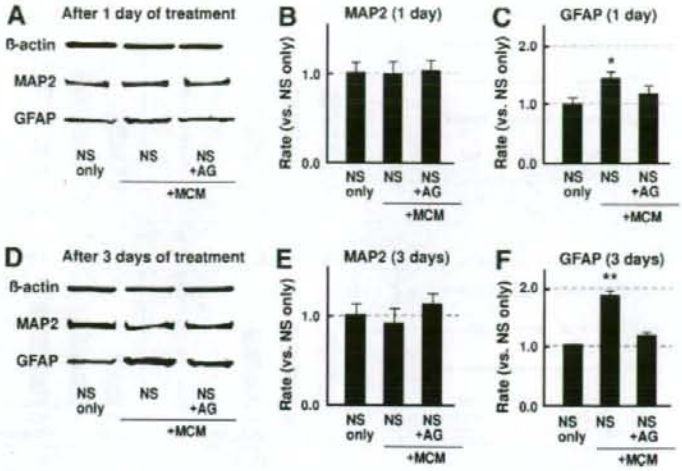

Figure 5. Effects of AG490 (AG) on NSCs cultured in MCM. After NSCs were seeded into 24-well plates at a density of 5.0×10^5/well, NSCs were incubated with MCM (conditioned medium from 24 h microglia cultures at a density of 1.4×10^5/ml) in the presence and absence of AG490 (a Jak2 kinase inhibitor; 1 μm/ml). One day (*A–C*) or 3 days later (*D–F*), the cells were homogenized in lysis buffer and immunoblotted with antibodies against GFAP or MAP2. Experiments were carried out 5 times independently. Note that microglia-induced astrogliogenesis was significantly inhibited by AG490. $^*P < 0.05$, $^{**}P < 0.01$ *vs.* NS only.

SOCS3, or LacZ (10 MOI each) and incubated with MCM (conditioned medium from 24 h microglia cultures at a density of 1.4×10^5/ml). Three days later, the cells were homogenized in lysis buffer and immunoblotted with an antibody against β-actin, SOCS3, Stat3, or pStat3 (Tyr705-phosphorylated Stat3).

Western blot analysis revealed that strong Stat3 and SOCS3 expression was evident in Ad.Stat3F- and Ad.SOCS3-infected cells but not in Ad.Lz-infected cells at 3 days after infection (**Fig. 7*A***). Stat3 protein was expressed in both Ad.Lz- and Ad.SOCS3-infected cells. Moreover, pStat3 was weakly expressed in Ad.Lz-infected cells, but expression of pStat3 was not evident in Ad.Stat3F- and Ad.SOCS3-infected cells (Fig. 7*A*). These data suggest that overexpression of Stat3F and SOCS3 could suppress Stat3 cell signaling in NSCs.

We next examined whether overexpression of Stat3F and SOCS3 could modulate the differentiation of NSCs. At 3 days after infection, cells were homogenized in lysis buffer and immunoblotted with an antibody against GFAP, MAP2, or Nestin (a marker of NSCs). Experiments were carried out 5 times independently.

Densitometric analysis revealed that 3 days after infection, MCM significantly increased the level of GFAP protein in Ad.LacZ-infected cells (~3.4-fold), whereas the level of MAP2 protein did not differ among all groups (Fig. 7*B, C*). Furthermore, the level of GFAP protein in Ad.Stat3F- and Ad.SOCS3-infected cells cultured with MCM was significantly reduced (~1.7- and 5.2-fold, respectively), compared with that in Ad.Lz-infected cells cultured with MCM (Fig. 7*B*). These results suggested that microglia-induced astrogliogenesis was inhibited by blocking the activation of endogenous Stat3 in NSCs.

In addition, densitometric analysis revealed that 3 days after infection, MCM significantly increased the level of Nestin protein in Ad.LacZ-infected cells (~1.4-fold; Fig. 7*D*). Furthermore, compared with that in Ad.Lz-infected cells cultured without MCM, the level of Nestin protein in Ad.SOCS3-infected cells cultured

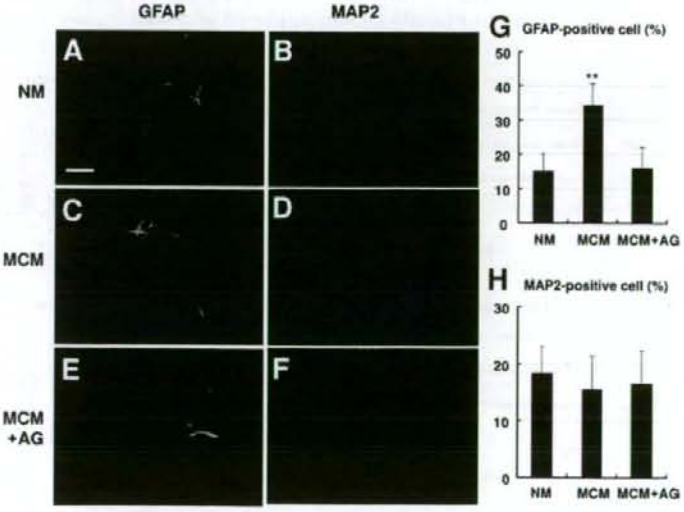

Figure 6. Effects of MCM on the fate of NSCs after 3 days of culture. After NSCs were seeded into 24-well plates at a density of 2.0×10^5/well, NSCs were incubated with neurosphere-differentiating medium (NM) or MCM in the presence or absence of AG490 (1 μm/ml). *A–F*) Three days later, expression of differentiation markers was evaluated by immunostaining with antibodies against GFAP (green; *A, C, E*) and MAP2 (red; *B, D, F*). To identify nuclei, cells were stained with Hoechst33342 (blue). Scale bar = 100 μm. Data were obtained from 5 independent measurements. Values represent means ± SD. *G*) GFAP-positive cells. *H*) MAP2-positive cells. $^{**}P < 0.01$ *vs.* NM. Note that MCM significantly increased the proportion of the GFAP-positive cells and this increase was inhibited by the treatment of AG490.

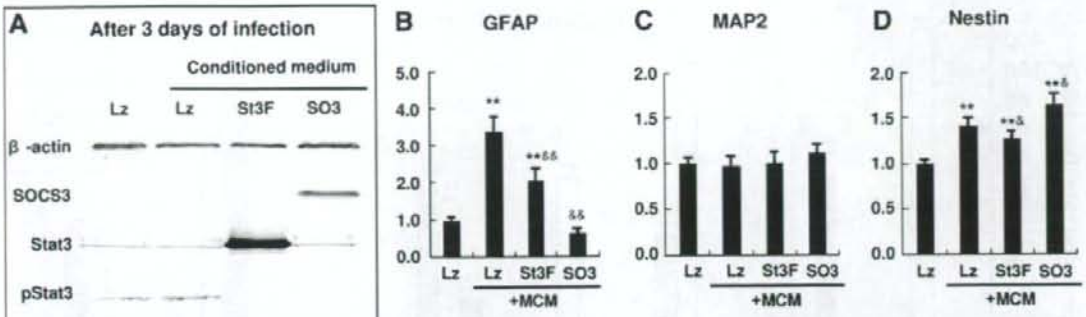

Figure 7. Effects of overexpression of Stat3F or SOCS3 on NSCs cultured in MCM. After NSCs were seeded into 24-well plates at a density of 5.0×10^5/well, NSCs were inoculated with adenovirus vector expressing Stat3F(St3F; a dominant negative form of Stat3), SOCS3(SO3), or LacZ(Lz) (10 MOI each) and incubated with MCM (conditioned medium from 24 h microglia cultures at a density of 1.4×10^5/ml). Three days later (*A*), the cells were homogenized in lysis buffer and immunoblotted with an antibody against β-actin, SOCS3, Stat3, pStat3 (Tyr705-phosphorylated Stat3), GFAP (*B*), MAP2 (*C*), or Nestin (*D*). Note that microglia-induced astrogliogenesis of NSCs was significantly inhibited by activation of endogenous Stat3 in NSCs. In addition, MCM significantly increased the protein level of Nestin in NSCs, and overexpression of SOCS3 induced an additional increase in Nestin protein. $^{**}P < 0.01$ *vs.* Lz; $^{\&}P < 0.05$, $^{\&\&}P < 0.01$ *vs.* Lz + MCM.

with MCM increased further (~1.6-fold; Fig. 7*D*). These results suggested that MCM promoted the maintenance of NSCs and SOCS3 accelerated this action.

Ramified microglial cells release neither NO nor inflammatory cytokines

To specify the properties of the microglial cells, we evaluated the amounts of NO and cytokines [interleukin (IL)-1β, IL-6, and TNF-α]. As shown in **Fig. 8*B–E***, microglial cells in neurosphere-differentiating medium without LPS released little amounts of NO and inflammatory cytokines. Moreover, the shape of these microglial cells was a ramified form (Fig. 8*A*).

Real-time PCR for trophic factors in neurons, astrocytes, microglial cells, and NSCs

Because microglia-induced astrogliogenesis in NSCs appeared to occur through paracrine effects, we next investigated mRNA levels of several secreted trophic factors that are considered to modulate the fate of NSCs. We compared mRNA levels of several trophic factors among neurons, astrocytes, microglial cells, and NSCs by real-time PCR. Data were obtained from 4 independent experiments. Among the trophic factors examined, the expression of LIF and FGF2 mRNA in microglial cells was markedly upregulated (~78.0- and 28.4-fold increase, respectively), compared with those in NSCs (**Fig. 9**). Furthermore, microglial cells did not express IL-6, CT1, BMP4, and EGF mRNA in our experimental conditions. These results suggested that LIF and FGF2 were involved in the mechanism of microglia-induced astrogliogenesis in NSCs and that microglial cells were not activated in our experimental conditions.

Promoter assay with and without MCM

To confirm whether MCM could actually activate Stat3 function in NSCs, minimal junB reporter constructs

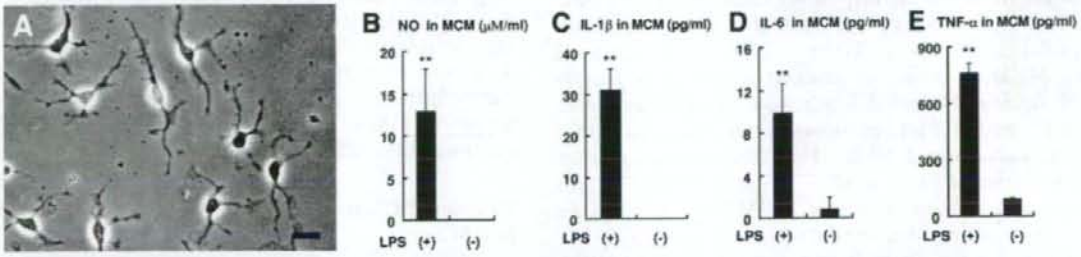

Figure 8. Properties of microglial cells. Microglial cells at a density of 4.0×10^5/ml were cultured for 24 h in neurosphere-differentiating medium. After their settlement was confirmed (*A*), cells were cultured with fresh neurosphere-differentiating media in the presence and absence of LPS (1 μg/ml). One day later, the concentrations of NO (*B*) and cytokines [IL-1β (*C*), IL-6 (*D*), and TNF-α (*E*)] in the supernatants were measured by Griess reaction and ELISA, respectively. Note the microglial cells displaying a ramified morphology (*A*; scale bar=25 μm). Note that microglial cells in neurosphere-differentiating medium without LPS released little amounts of NO (*B*) and inflammatory cytokines [IL-1β (*C*), IL-6 (*D*), and TNF-α (*E*)]. $^{**}P < 0.01$ *vs.* LPS(−).

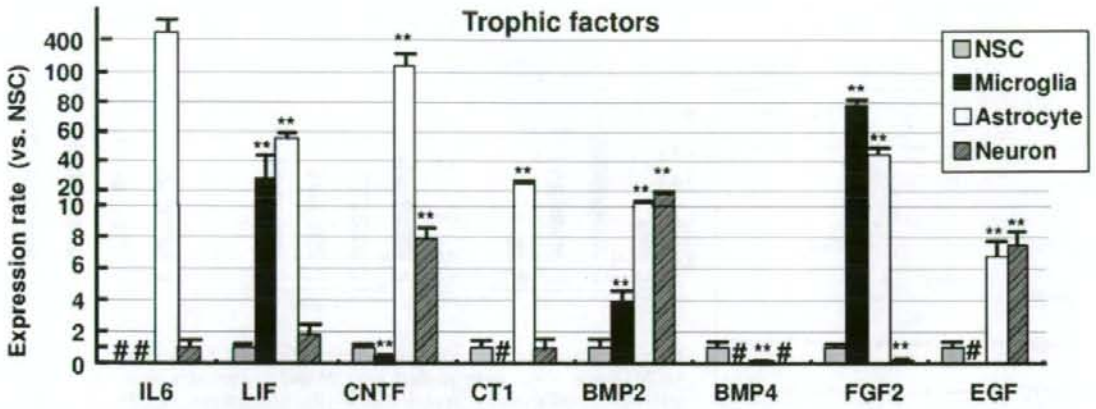

Figure 9. Expression of trophic factors in neurons, astrocytes, microglial cells, and NSCs. Cultured neurons, astrocytes, microglial cells, and NSCs were washed with PBS, and total RNA was extracted using Isogen (Nippon Gene). Total RNA was digested with DNase, and then single stranded cDNA was obtained using oligo dT primers and Moloney murine leukemia virus reverse transcriptase (Life Technologies). For quantitative real-time PCR, TaqMan real-time PCR analysis was carried out. The oligonucleotide primers and TaqMan fluorogenic probe for each gene were purchased commercially (Applied Biosystems; Table 1). The mRNA levels of several trophic factors were compared among neurons, astrocytes, microglial cells, and NSCs by real-time PCR. Data were obtained from 4 independent experiments. Note that expression of LIF and FGF2 in microglial cells was significantly upregulated, compared with that in NSCs. $^{**}P < 0.01$ *vs.* NSC; #not detected.

with or without 4 copies of APRE were electroporated into the neurospheres. Then, the neurospheres were exposed to adenoviral vectors expressing SOCS3, Stat3F, or LacZ in the presence and absence of MCM. Two days later, dual luciferase assay was carried out. Experiments were carried out 5 times independently. After transfection of the Stat3 reporter plasmid (minimal junB promoter with 4 copies of APRE), relative luciferase activity in Ad.LacZ-, Ad.Stat3F-, Ad SOCS3- and Ad.LacZ + LIF + FGF2-treated NSCs cultured with MCM was significantly increased (~35.9-, 2.4-, 3.0-, and 2.0-fold, respectively) compared to that in Ad.LacZ-, Ad.Stat3F-, Ad.SOCS3-, and Ad.LacZ + LIF + FGF2-treated NSCs cultured without MCM, respectively (**Fig. 10*A***). When NSCs were cultured without MCM, relative luciferase activity of Ad.Stat3F- and Ad.SOCS3-treated NSCs was significantly lower (~1.7- and 1.8-fold, respectively) than that of Ad.LacZ-treated NSCs, whereas relative luciferase activity of Ad.LacZ + LIF + FGF2-treated NSCs was significantly higher than that of Ad-.LacZ-treated NSCs. When NSCs were cultured with MCM, the relative luciferase activity of Ad.Stat3F- and Ad.SOCS3-treated NSCs was significantly lower (~26.1- and 21.9-fold reduction, respectively) than that of Ad.LacZ-treated NSCs (Fig. 10*A*). However, after transfection of Stat3 control plasmid (minimal junB promoter without 4 copies of APRE), the relative luciferase activity did not differ among all groups (Fig. 10*B*). Taken together, these results proved that MCM, as well as treatment with LIF + FGF2, transactivated APRE and promoted Stat3 function. We also confirmed that overexpression of Stat3F and SOCS3 inhibited APRE transactivation *via* MCM and blocked Stat3 function.

Real-time PCR for Notch family members and inhibitory basic helix-loop-helix (bHLH) factors

Notch family members and inhibitory bHLH transcription factors play an important role in proliferation, cell lineage determination, and cell differentiation of NSCs (16). We therefore examined the effects of MCM on the mRNA levels of Notch family members (notch1, 2, and 3) as well as inhibitory bHLH transcription factors (hes1, hes5, id1, id2, and id3) in NSCs in the presence or absence of AG490. The mRNA levels in NSCs were evaluated using real-time PCR at 1 day after culture with MCM. Data were obtained from 4 independent experiments.

One day after culture with MCM, the mRNA levels of notch1–3, hes5, and id3 in NSCs were significantly increased (~3.4-, 1.8-, 2.5-, 1.4-, and 4.7-fold, respectively), compared with those in NSCs without MCM (**Fig. 11*A***). Furthermore, after treatment with AG490, the mRNA levels of notch1, 2, and 3 in NSCs were significantly decreased (~1.6-, 1.5-, and 1.4-fold, respectively), whereas the mRNA level of hes5 was significantly increased further (~1.4-fold). Irrespective of treatment with AG490, the mRNA level of id3 in NSCs cultured with MCM was not changed.

Real-time PCR for proneural bHLH factors and Sox9 in NSCs

Proneural bHLH factors have been reported to block astrocyte differentiation (17), and in their absence, neural progenitors become astrocytes (18). On the contrary, Sox9 plays a crucial role in causing NSCs to switch from neurogenesis to gliogenesis (19). For these

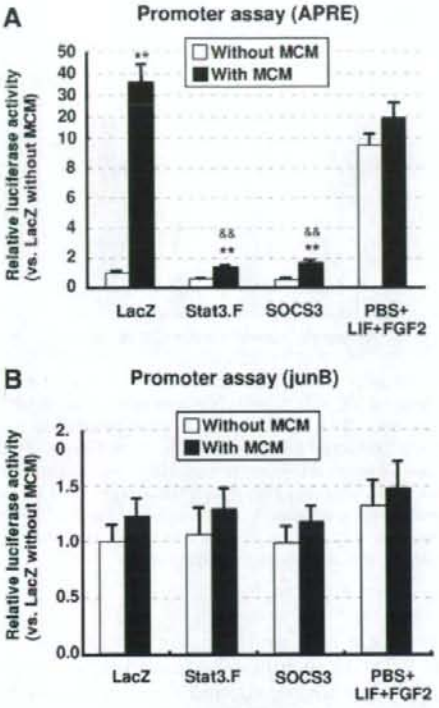

Figure 10. Activation of Stat3 function in NSCs mediated by MCM. Minimal junB reporter constructs with (*A*) or without (*B*) 4 copies of APRE were electroporated into the neurospheres. Then NSCs cultured with MCM were exposed to adenoviral vectors expressing SOCS3, Stat3F, or LacZ. Two days later, dual luciferase assay was carried out. Experiments were carried out 5 times independently. Note that MCM, as well as treatment with LIF + FGF2, transactivated APRE and promoted Stat3 function. Furthermore, overexpression of Stat3F and SOCS3 inhibited APRE transactivation *via* MCM and blocked Stat3 function. $^{**}P < 0.01$ *vs.* without MCM; $^{\&\&}P < 0.01$ *vs.* LacZ with MCM.

reasons, we examined the effects of MCM on the mRNA levels of proneural bHLH factors (mash1, neuroD1, and neuroD2) and sox9 in NSCs.

One day after culture with MCM, mRNA levels of mash1, neuroD1, and neuroD2 were significantly decreased in NSCs (~1.9-, 1.4-, and 1.6-fold, respectively), whereas the mRNA level of Sox9 was significantly increased in NSCs (~1.3-fold; Fig. 11*B*). Treatment with AG490 significantly decreased mRNA levels of neuroD2 and sox9 (~1.6- and 2.0-fold, respectively) in NSCs cultured with MCM.

DISCUSSION

In the present study, we prepared three types of coculture of NSCs with microglial cells: mixed type, insert type, and conditioned type. In all types, microglial cells promoted astrogliogenesis, suggesting that their effects were not caused by physical contact between the two cell populations but by some diffusible factors released by microglial cells. Our results differed from previous reports (20, 21) that microglial cells promoted neurogenesis in adult NSCs. One possible explanation is the difference in NSCs (*i.e.*, embryonic NSCs from the ganglionic eminences were used in our study whereas adult NSCs from the subventricular zone or the hippocampus were used in their studies). Another possible explanation is that the condition of microglial cells was different. It has been reported that both interferon-γ- and IL-4-activated microglial cells promoted neurogenesis of adult NSCs whereas LPS-activated microglial cells inhibited this neurogenesis (22). Moreover, macrophage colony-stimulating factor (M-CSF) -activated microglial cells promoted astrogliogenesis of NSCs (23). In our study, microglial cells were not activated by cytokines (such as interferon-γ and IL-4) or LPS. Consequently, IL-6 mRNA was not detected in microglial cells and little amounts of NO and inflammatory cytokines, such as IL-1β, IL-6, and TNF-α were detected in the conditioned medium. Furthermore, these microglia cells were displaying a ramified morphology. Thus, we demonstrated that ramified microglial cells promoted astrogliogenesis through their paracrine effects.

To investigate the cell signaling pathways of this microglia-induced astrogliogenesis of NSCs, we applied four types of reagents to inhibit the cell signaling for modulating the fate of NSCs. Consequently, a PI3K inhibitor (LY294002), a BMP-specific antagonist (Noggin), and an SHP inhibitor (PTP inhibitor II) did not inhibit this astrogliogenesis. Among them, only the Jak2 kinase inhibitor (AG490) inhibited microglia-induced astrogliogenesis in NSCs, suggesting a crucial role of the Jak-Stat signaling pathway in this mechanism. Subsequent studies, using adenovirus vectors, revealed that Stat3 (especially gp130 signaling) played a pivotal role in microglia-induced astrogliogenesis of NSCs. It is well known that Stat3 plays crucial roles in determining the fate of NSCs. Enhancement of Stat3 activity in NSCs leads to subsequent glial differentiation (14). LIF as well as ciliary neurotrophic factor (CNTF) and IL-6 can activate the Jak-Stat signaling pathway and promote astroglial differentiation (24). Phosphorylated Stat3 associates with the transcriptional coactivators CREB-binding protein (CBP/p300) to activate expression of astrocyte-specific genes (25). DNA methylation is also a critical determinant in the developmental stage-dependent regulation of astrocytogeneis (26). In this study, we showed that the level of LIF mRNA in microglial cells was significantly higher than that in NSCs, although the level of CNTF mRNA in microglial cells was significantly lower than that in NSCs, and neither IL-6 mRNA nor CT1 mRNA was detected in microglial cells. These data suggested that ramified microglial cells secreted LIF and promoted astrogliogenesis in NSCs.

We also showed that the level of FGF2 mRNA in microglial cells was significantly greater than that in NSCs. FGF2 was first purified as a heparin-binding polypeptide from bovine pituitary and was subsequently

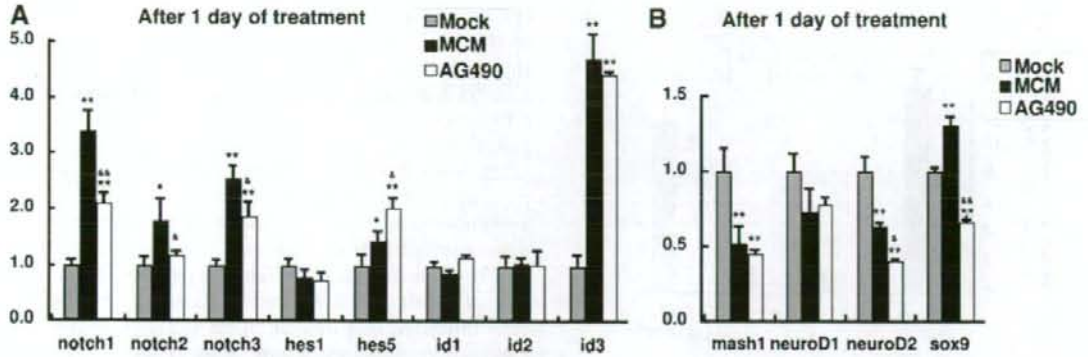

Figure 11. mRNA expression profiles of notch family, bHLH factors, or sox9 after 1 day of treatment with MCM in the presence or absence of AG490. After NSCs were seeded into 24-well plates at a density of 5.0×10^5/well, NSCs were incubated with MCM in the presence and absence of AG490 (a Jak2 kinase inhibitor; 1 μm/ml). As a control, NSCs were incubated only with neurosphere-differentiating medium (mock). One day later, total RNA was extracted using Isogen (Nippon Gene). Total RNA was digested with DNase, and then single-stranded cDNA was obtained using oligo dT primers and Moloney murine leukemia virus reverse transcriptase (Life Technologies). For quantitative real-time PCR, TaqMan real-time PCR analysis was carried out. The oligonucleotide primers and TaqMan fluorogenic probe for each gene were purchased commercially (Applied Biosystems; Table 1). Data were obtained from 4 independent experiments. Note that expression of notch1–3 (*A*) and sox9 (*B*) was significantly upregulated after treatment with MCM, and this up-regulation was significantly inhibited by AG490. $^{*}P < 0.05$, $^{**}P < 0.01$ *vs.* Mock; $^{\&}P < 0.05$, $^{\&\&}P < 0.01$ *vs.* MCM.

characterized as a basic protein of 18 kDa (27). FGF-2 is a strong promoter of fibroblast proliferation. However, most of the interest in FGF-2 stems from its pleiotropic effects. FGF-2 is one of the most potent angiogenic factors, possesses neuroprotective properties, and is implicated in vascular remodeling and tumor metastasis (28). It has been shown that the *in vitro* expansion and differentiation of NSCs can be regulated by adding FGF2 to the culture medium (29). Moreover, it has been reported that FGF2 is expressed in the dorsolateral cortical neuroepithelium of the forebrain and FGF2 is one of the most potent mitogens and survival factors for cultured NSCs (30). As well as FGF-2, LIF is also known to be required for long-term maintenance of NSCs (31). In our study, we demonstrated that the level of Nestin protein in NSCs was significantly increased by treatment with MCM, suggesting that ramified microglia-derived LIF and FGF2 promoted the maintenance of NSCs.

To clarify the molecular mechanisms underlying microglia-induced astrogliogenesis, we investigated the expression of Notch family members bHLH transcription factors, and sox9 genes. Notch family members and bHLH transcription factors play important roles in proliferation, cell lineage determination and cell differentiation of NSCs (16). Several investigators have shown interactions between the Stat3 and Notch pathways. It has been reported that activation of glycoprotein 130 (gp130; a common receptor component of IL-6 family cytokines) stimulates the Notch1 pathway, increasing the expression of hairy-enhancer-of-split 1 (Hes1; ref. 32). It has also been demonstrated that Stat3 is an essential effector of Notch-Hes signaling (33). Furthermore, it has been reported that the notch ligand delta-like 1 (DLL1) is a key target of Stat3 in both inhibition of neurogenesis and maintenance of NSCs, which may underlie the noncell-autonomous action of Stat3 in inhibiting neuronal differentiation (34). In this study, we showed significant up-regulation of notch 1, 2, and 3 mRNA at 1 day after treatment with MCM, and this up-regulation was significantly inhibited by the Jak2 inhibitor, AG490, whereas hes1 and hes5 mRNA were not. We cannot explain why the temporal profiles of hes1 and hes5 mRNA (downstream genes of notch signaling) were not the same as those of notch1–3 mRNA. However, neurospheres could be generated from embryos mutant for hes1 and hes5. Hes1 and hes5 double-mutant neurospheres still demonstrated self-renewal (35). It has also been reported that neither hes1 nor hes5 mediates gp-130-enhanced notch signaling that regulates NSC maintenance (32). These results support the contention that besides the Notch-Hes pathway other signaling pathways can mediate notch signaling in the maintenance and differentiation of NSCs.

In addition, it is well known that Sox9 plays a crucial role in chondrocyte development and male sex determination (36). Recently, it has been demonstrated that Sox9 is essential for proper development of both oligodendrocytes and astrocytes and suggested that Sox9 is a component of the mechanism that causes NSCs to switch from neurogenesis to gliogenesis (19). Sox9 has also been implicated in maintaining cells in a stem cell-like state and preventing their exit from the cell cycle and the induction of neurogenesis (37). Furthermore, notch signaling is required for the maintenance of Sox9 expression during the gliogenic phase of spinal cord development (38). Consistent with these previous reports, our data showed that MCM-induced up-regulation of sox9 and notch1–3 promotes astrogliogenesis and maintenance of NSCs.

In conclusion, we have demonstrated that ramified

microglial cells promote astrogliogenesis and maintenance of NSCs through their paracrine effects and that their effects are caused by activation of Stat3 function. This finding of active roles of microglial cells is unexpected and raises the possibility that neuronal production in the brain is regulated, at least in part, by the regional properties of microglial cells. FJ

REFERENCES

1. Alvarez-Buylla, A., and Lim, D. A. (2004) For the long run: maintaining germinal niches in the adult brain. *Neuron* **41,** 683–686
2. Song, H., Stevens, C. F., and Gage, F. H. (2002) Astroglia induce neurogenesis from adult neural stem cells. *Nature* **417,** 39–44
3. Aarum, J., Sandberg, K., Haeberlein, S. L., and Persson, M. A. (2003) Migration and differentiation of neural precursor cells can be directed by microglia. *Proc. Natl. Acad. Sci. U. S. A.* **100,** 15983–15988
4. Ziv, Y., Ron, N., Butovsky, O., Landa, G., Sudai, E., Greenberg, N., Cohen, H., Kipnis, J., and Schwartz, M. (2006) Immune cells contribute to the maintenance of neurogenesis and spatial learning abilities in adulthood. *Nat. Neurosci.* **9,** 268–275
5. Aloisi, F. (2001) Immune function of microglia. *Glia* **36,** 165–179
6. Streit, W. J. (2002) Microglia as neuroprotective, immunocompetent cells of the CNS. *Glia* **40,** 133–139
7. Polazzi, E., and Contestabile, A. (2002) Reciprocal interactions between microglia and neurons: from survival to neuropathology. *Rev. Neurosci.* **13,** 221–242
8. Suzumura, A., Mezitis, S. G., Gonatas, N. K., and Silberberg, D. H. (1987) MHC antigen expression on bulk isolated macrophage-microglia from newborn mouse brain: induction of Ia antigen expression by gamma-interferon. *J. Neuroimmunol.* **15,** 263–278
9. Cao, F., Hata, R., Zhu, P., Ma, Y. J., Tanaka, J., Hanakawa, Y., Hashimoto, K., Niinobe, M., Yoshikawa, K., and Sakanaka, M. (2006) Overexpression of SOCS3 inhibits astrogliogenesis and promotes maintenance of neural stem cells. *J. Neurochem.* **98,** 459–470
10. Gu, F., Hata, R., Ma, Y. J., Tanaka, J., Mitsuda, N., Kumon, Y., Hanakawa, Y., Hashimoto, K., Nakajima, K., and Sakanaka, M. (2005) Suppression of Stat3 promotes neurogenesis in cultured neural stem cells. *J. Neurosci. Res.* **81,** 163–171
11. Kanegae, Y., Makimura, M., and Saito, I. (1994) A simple and efficient method for purification of infectious recombinant adenovirus. *Jpn. J. Med. Sci. Biol.* **47,** 157–166
12. Laemmli, U. K. (1970) Cleavage of structural proteins during the assembly of the head of bacteriophage T4. *Nature* **227,** 680–685
13. Livak, K. J., and Schmittgen, T. D. (2001) Analysis of relative gene expression data using real-time quantitative PCR and the 2[-Delta Delta C(T)] method. *Methods* **25,** 402–408
14. Rajan, P., and McKay, R. D. (1998) Multiple routes to astrocytic differentiation in the CNS. *J. Neurosci.* **18,** 3620–3629
15. Schmitz, J., Weissenbach, M., Haan, S., Heinrich, P. C., and Schaper, F. (2000) SOCS3 exerts its inhibitory function on interleukin-6 signal transduction through the SHP2 recruitment site of gp130. *J. Biol. Chem.* **275,** 12848–12856
16. Lasky, J. L., and Wu, H. (2005) Notch signaling, brain development, and human disease. *Pediatr. Res.* **57,** 104R–109R
17. Sun, Y., Nadal-Vicens, M., Misono, S., Lin, M. Z., Zubiaga, A., Hua, X., Fan, G., and Greenberg, M. E. (2001) Neurogenin promotes neurogenesis and inhibits glial differentiation by independent mechanisms. *Cell* **104,** 365–376
18. Nieto, M., Schuurmans, C., Britz, O., and Guillemot, F. (2001) Neural bHLH genes control the neuronal versus glial fate decision in cortical progenitors. *Neuron* **29,** 401–413
19. Stolt, C. C., Lommes, P., Sock, E., Chaboissier, M. C., Schedl, A., and Wegner, M. (2003) The Sox9 transcription factor determines glial fate choice in the developing spinal cord. *Genes Dev.* **17,** 1677–1689
20. Battista, D., Ferrari, C. C., Gage, F. H., and Pitossi, F. J. (2006) Neurogenic niche modulation by activated microglia: transforming growth factor beta increases neurogenesis in the adult dentate gyrus. *Eur. J. Neurosci.* **23,** 83–93
21. Walton, N. M., Sutter, B. M., Laywell, E. D., Levkoff, L. H., Kearns, S. M., Marshall, G. P., 2nd, Scheffler, B., and Steindler, D. A. (2006) Microglia instruct subventricular zone neurogenesis. *Glia* **54,** 815–825
22. Butovsky, O., Ziv, Y., Schwartz, A., Landa, G., Talpalar, A. E., Pluchino, S., Martino, G., and Schwartz, M. (2006) Microglia activated by IL-4 or IFN-gamma differentially induce neurogenesis and oligodendrogenesis from adult stem/progenitor cells. *Mol. Cell. Neurosci.* **31,** 149–160
23. Nakanishi, M., Niidome, T., Matsuda, S., Akaike, A., Kihara, T., and Sugimoto, H. (2007) Microglia-derived interleukin-6 and leukaemia inhibitory factor promote astrocytic differentiation of neural stem/progenitor cells. *Eur. J. Neurosci.* **25,** 649–658
24. Bonni, A., Sun, Y., Nadal-Vicens, M., Bhatt, A., Frank, D. A., Rozovsky, I., Stahl, N., Yancopoulos, G. D., and Greenberg, M. E. (1997) Regulation of gliogenesis in the central nervous system by the JAK-STAT signaling pathway. *Science* **278,** 477–483
25. Nakashima, K., Yanagisawa, M., Arakawa, H., Kimura, N., Hisatsune, T., Kawabata, M., Miyazono, K., and Taga, T. (1999) Synergistic signaling in fetal brain by STAT3-Smad1 complex bridged by p300. *Science* **284,** 479–482
26. Taga, T., and Fukuda, S. (2005) Role of IL-6 in the neural stem cell differentiation. *Clin. Rev. Allergy Immunol.* **28,** 249–256
27. Abraham, J. A., Mergia, A., Whang, J. L., Tumolo, A., Friedman, J., Hjerrild, K. A., Gospodarowicz, D., and Fiddes, J. C. (1986) Nucleotide sequence of a bovine clone encoding the angiogenic protein, basic fibroblast growth factor. *Science* **233,** 545–548
28. Yu, P. J., Ferrari, G., Galloway, A. C., Mignatti, P., and Pintucci, G. (2007) Basic fibroblast growth factor (FGF-2): the high molecular weight forms come of age. *J. Cell. Biochem.* **100,** 1100–1108
29. Gage, F. H., Coates, P. W., Palmer, T. D., Kuhn, H. G., Fisher, L. J., Suhonen, J. O., Peterson, D. A., Suhr, S. T., and Ray, J. (1995) Survival and differentiation of adult neuronal progenitor cells transplanted to the adult brain. *Proc. Natl. Acad. Sci. U. S. A.* **92,** 11879–11883
30. Dono, R. (2003) Fibroblast growth factors as regulators of central nervous system development and function. *Am. J. Physiol. Regul. Integr. Comp. Physiol.* **284,** R867–R881
31. Shimazaki, T., Shingo, T., and Weiss, S. (2001) The ciliary neurotrophic factor/leukemia inhibitory factor/gp130 receptor complex operates in the maintenance of mammalian forebrain neural stem cells. *J. Neurosci.* **21,** 7642–7653
32. Chojnacki, A., Shimazaki, T., Gregg, C., Weinmaster, G., and Weiss, S. (2003) Glycoprotein 130 signaling regulates Notch1 expression and activation in the self-renewal of mammalian forebrain neural stem cells. *J. Neurosci.* **23,** 1730–1741
33. Kamakura, S., Oishi, K., Yoshimatsu, T., Nakafuku, M., Masuyama, N., and Gotoh, Y. (2004) Hes binding to STAT3 mediates crosstalk between Notch and JAK-STAT signalling. *Nat. Cell Biol.* **6,** 547–554
34. Yoshimatsu, T., Kawaguchi, D., Oishi, K., Takeda, K., Akira, S., Masuyama, N., and Gotoh, Y. (2006) Non-cell-autonomous action of STAT3 in maintenance of neural precursor cells in the mouse neocortex. *Development* **133,** 2553–2563
35. Ohtsuka, T., Sakamoto, M., Guillemot, F., and Kageyama, R. (2001) Roles of the basic helix-loop-helix genes Hes1 and Hes5 in expansion of neural stem cells of the developing brain. *J. Biol. Chem.* **276,** 30467–30474
36. Bi, W., Deng, J. M., Zhang, Z., Behringer, R. R., and de Crombrugghe, B. (1999) Sox9 is required for cartilage formation. *Nat. Genet.* **22,** 85–89
37. Seymour, P. A., Freude, K. K., Tran, M. N., Mayes, E. E., Jensen, J., Kist, R., Scherer, G., and Sander, M. (2007) SOX9 is required for maintenance of the pancreatic progenitor cell pool. *Proc. Natl. Acad. Sci. U. S. A.* **104,** 1865–1870
38. Taylor, M. K., Yeager, K., and Morrison, S. J. (2007) Physiological Notch signaling promotes gliogenesis in the developing peripheral and central nervous systems. *Development* **134,** 2435–2447

Received for publication January 15, 2008.
Accepted for publication July 2, 2008.

Baseline NIH Stroke Scale Score predicting outcome in anterior and posterior circulation strokes

S. Sato, MD
K. Toyoda, MD
T. Uehara, MD
N. Toratani, MD
C. Yokota, MD
H. Moriwaki, MD
H. Naritomi, MD
K. Minematsu, MD

Address correspondence and reprint requests to Dr. Kazunori Toyoda, Cerebrovascular Division, Department of Medicine, National Cardiovascular Center, 5-7-1 Fujishirodai, Suita, Osaka 565-8565, Japan
toyoda@hsp.ncvc.go.jp

ABSTRACT

Objective: The NIH Stroke Scale (NIHSS) may not appropriately assess the spectrum of posterior circulation (PC)-related neurologic deficits. We determined the cutoff baseline NIHSS score that predicts independent daily life activity during the chronic stage in anterior circulation (AC) vs PC ischemic strokes.

Methods: A total of 310 consecutive patients hospitalized within 3 days after the onset of an ischemic stroke were prospectively enrolled in the study. Patients on thrombolytic therapy were excluded. In all patients, infarcts and vascular lesions were identified primarily using magnetic resonance techniques. A favorable outcome was defined as a modified Rankin Scale score of ≤2 at 3 months poststroke.

Results: In 101 patients with PC stroke, the total baseline NIHSS score was lower ($p < 0.001$), and the subscores of ataxia ($p < 0.001$) and visual fields ($p = 0.043$) were higher than in 209 patients with AC stroke. Multivariate-adjusted OR for the favorable outcome in patients with PC vs AC stroke was 2.339 (95% CI 1.331–4.109, $p = 0.003$). A low baseline NIHSS score was independently predictive of a favorable outcome in both patients with PC (OR 1.547, 95% CI 1.232–1.941) and AC (1.279, 1.188–1.376) stroke. The optimal cutoff scores of the baseline NIHSS for the favorable outcome were ≤5 for patients with PC stroke (sensitivity, 84%; specificity, 81%) and ≤8 for patients with AC stroke (sensitivity, 80%; specificity, 82%).

Conclusions: The cutoff score of the baseline NIH Stroke Scale (NIHSS) for a favorable chronic outcome was relatively low in patients with PC stroke compared to patients with AC stroke. The NIHSS appears to have limitations with respect to its use when comparing the neurologic severity of PC and AC stroke. ***Neurology*® 2008;70:1-1**

GLOSSARY

AC = anterior circulation; **AUC** = area under the ROC curve; **mRS** = modified Rankin Scale; **NIHSS** = NIH Stroke Scale; **OCSP** = Oxfordshire Community Stroke Project; **PC** = posterior circulation; **ROC** = receiver operating characteristic; **rt-PA** = recombinant tissue plasminogen activator; **TOAST** = Trial of ORG 10172 in Acute Stroke Treatment.

The NIH Stroke Scale (NIHSS) is a neurologic severity scale that is valid, reliable, and reproducible[1-4]; it is commonly used in many clinical trials dealing with medical therapy for acute stroke.[5,6] Baseline NIHSS scores on admission are associated with chronic functional outcome,[6-8] hospital disposition after stroke,[9,10] infarct volume, and angiographic findings.[11-13]

In the Trial of ORG 10172 in Acute Stroke Treatment (TOAST), the baseline NIHSS score was lower in patients with posterior circulation (PC) stroke than in patients with anterior circulation (AC) stroke.[14] In a single-center study of Chinese patients with stroke, a severe baseline NIHSS score (≥9) was less frequent in patients with PC stroke than in patients with other stroke subtypes determined according to the Oxfordshire Community Stroke Project (OCSP) classification.[15] These results foretell that the long-term chronic outcome was also better in patients with PC stroke than in patients with AC

e-Pub ahead of print at www.neurology.org.
From the Cerebrovascular Division, Department of Medicine, National Cardiovascular Center, Suita, Osaka, Japan.
Supported in part by Grants-in-Aid from the Ministry of Health, Labor and Welfare, Japan (H18-Junkanki-044).
Disclosure: The authors report no disclosures.

stroke. In fact, in the TOAST study, a favorable outcome at 3 months was more common in patients with PC stroke than in patients with AC stroke, although the outcome was no longer different after adjusting for confounders, including the baseline NIHSS score.[14] It has been reported that a favorable outcome was more common in patients with PC stroke (71%) than in patients with a partial (58%) or a total (3%) AC stroke.[16] These studies using quantitative scales have shown that, unlike what has previously been thought,[17] patients with PC stroke do not have a poorer prognosis than patients with AC stroke. However, these results highlight the important issue of whether the NIHSS is valid for comparing the neurologic severity of AC and PC stroke.

To resolve this issue, we assessed the NIHSS score on admission and the chronic outcome at 3 months, as well as the underlying clinical characteristics, of consecutive patients with stroke in a single stroke center. The aim of the present study was to compare how the baseline NIHSS score predicts chronic outcome in AC and PC ischemic stroke.

METHODS The study had a prospective observational cohort design. Patients who were admitted to our stroke center from December 2004 through December 2005 were enrolled. A total of 387 consecutive patients with acute ischemic stroke who were hospitalized within 3 days after symptom onset were registered. Of them, the following 77 patients were ineligible and were excluded from the study: 1) those receiving intra-arterial (3 patients) or IV (7 patients) thrombolytic therapy (all for the AC stroke); 2) those who were dependent with respect to their activities of daily living prior to the stroke (corresponding to a modified Rankin Scale [mRS] score of ≥ 3: 29 patients); 3) those with fresh ischemic lesions in both AC and PC territories (29 patients); 4) those with no relevant ischemic lesion on brain imaging (9 patients). The Regional Ethics and Hospital Management Committees approved the study. Written informed consent to participate in the study was obtained from the patient whenever possible; assent from a relative was obtained if patients could not consent themselves.

Baseline data were collected for all eligible patients, including gender, age, comorbidities, and neurologic deficits using the NIHSS on admission. The NIHSS subitems were also analyzed. The functional outcome was assessed at 3 months using the mRS determined by clinical examination (or by a mail-in survey for patients with too severe neurologic deficits to visit the clinic). A favorable outcome was defined as a mRS score of 0 to 2 (patients can look after their own affairs without assistance). The outcome corresponding to mRS score of 0 to 1 (patients can carry out all usual duties and activities) was also assessed. Death was coded as mRS 6. All patients had 12-lead electrocardiography, 72-hour electrocardiography monitoring, and transthoracic or transesophageal echocardiography. The location of infarcts was principally verified by diffusion-weighted MRI. In 11 patients for whom MRI was contraindicated, the fresh infarct was identified using repeated CT. In all patients, vascular lesions were verified by MRA (unless contraindicated) and carotid duplex sonography; conventional angiography was performed if needed. Stroke subtype was classified according to the TOAST categories.[18]

Statistical analysis was performed using the SPSS 11.0J statistical software package (SPSS Inc.). Between patients with AC and PC stroke, baseline clinical characteristics were compared using χ^2 tests and unpaired t tests, and NIHSS subscores were analyzed using the Mann-Whitney U test. OR for the favorable functional outcome in overall patients, corresponding to the mRS score of 0 to 2, according to the location of infarcts was determined using univariate or multivariate logistic regression analyses after adjustment for age, gender, and stroke subtypes (established clinical determinants of the stroke outcome). The baseline NIHSS score, another known determinant of the stroke outcome, was not used for the adjustment because we premised that the scale treats PC and AC strokes differently. To identify independent predictors for favorable outcome in patients with AC stroke and PC stroke separately, multivariate logistic regression analyses were performed using age, gender, stroke subtype, baseline NIHSS score, and the risk factors and comorbidities that showed the association with $p < 0.15$ in the univariate logistic regression analyses for patients with either AC or PC stroke. To obtain the baseline NIHSS score as the cutoff point for discriminating between patients with a favorable outcome and those without, we constructed receiver operating characteristic (ROC) curves and calculated the area under the ROC curve (AUC) with 95% CIs. $p < 0.05$ was considered significant.

RESULTS A total of 310 patients (202 men, 108 women; aged 71 ± 11 years) were enrolled in this study. A total of 209 patients had infarcts in the AC territory; 101 had infarcts in the PC territory.

Clinical characteristics of patients are presented in table 1 and figure 1. Patients with PC stroke were younger than patients with AC stroke ($p = 0.008$). There were no significant differences between the two groups in gender, comorbidities, or stroke subtypes. The baseline NIHSS score ($p < 0.001$) and the mRS at 3 months ($p = 0.001$) were lower in patients with PC stroke than in patients with AC stroke. Compared with patients with AC stroke, the unadjusted OR for the mRS score of 0 to 2 in patients with PC stroke was 2.313 (95% CI 1.371–3.901, $p = 0.002$), and the multivariate-adjusted OR was 2.339 (95% CI 1.331–4.109, $p = 0.003$).

Table 1 Patient demographics, comorbidities, baseline NIH Stroke Scale (NIHSS), and chronic outcome

	Anterior circulation (n = 209)	Posterior circulation (n = 101)	p Value
Demographics			
Age, y	72 ± 10	68 ± 12	0.008
Gender, male, n (%)	135 (65)	67 (66)	0.800
Comorbidities, n (%)			
Previous stroke	59 (28)	31 (33)	0.403
Hypertension	152 (73)	71 (70)	0.687
Diabetes mellitus	65 (31)	39 (39)	0.201
Hyperlipidemia	83 (40)	36 (36)	0.534
Ischemic heart disease	39 (19)	16 (16)	0.635
Valvular heart disease	15 (7)	9 (9)	0.652
Atrial fibrillation	77 (37)	33 (33)	0.527
Peripheral artery disease	15 (7)	5 (5)	0.623
Stroke subtype, n (%)			0.160
Small-vessel	35 (17)	15 (15)	
Cardioembolism	92 (44)	34 (34)	
Large-artery	33 (16)	25 (25)	
Other/undetermined	49 (23)	27 (27)	
Baseline NIHSS score, median (interquartile range)	8 (4–15)	4 (2–7)	<0.001
mRS score at 3 months, median (interquartile range)	2 (1–4)	1 (1–3)	0.001

mRS = modified Rankin Scale.

Table 2 shows the distribution of individual baseline NIHSS subscores. Items of the NIHSS score for ataxia and visual fields were higher in patients with PC stroke than in patients with AC stroke. Most of the other NIHSS item scores, such as level of consciousness, gaze, facial palsy, motor arm, motor leg, language, and extinction/inattention, were higher in patients with AC stroke than in patients with PC stroke.

Figure 1 Distribution of the baseline NIH Stroke Scale (NIHSS) score and modified Rankin Scale (mRS) score at 3 months

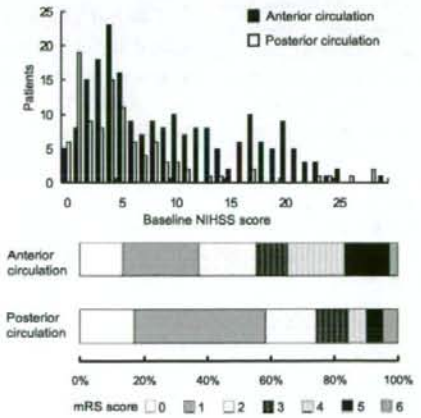

Univariate and multivariate analyses done to determine predictors of a favorable chronic outcome are shown in table 3. A lower baseline NIHSS score was independently predictive of a favorable outcome for patients with AC (OR 1.279, 95% CI 1.188–1.376) and PC (OR 1.547, 95% CI 1.232–1.941) stroke. In addition, ischemic heart disease was independently predictive of an unfavorable outcome (mRS 3–6) in patients with PC stroke.

The AUC of the ROC curve for predicting a favorable outcome, corresponding to mRS of 0 to 2, in patients with PC stroke (0.867, 95% CI 0.783–0.951) was similar to that in patients with AC stroke (0.868, 95% CI 0.818–0.917, figure 2). For patients with PC stroke, the optimal cutoff score of the baseline NIHSS was ≤5 with a sensitivity of 84% (95% CI 74–92%), specificity of 81% (61–93%), positive predictive value of 93% (84–98%), and negative predictive value of 64% (45–80%). For patients with AC stroke, the optimal cutoff score was ≤8 with a sensitivity of 80% (95% CI 72–87%), specificity of 82% (72–89%), positive predictive value of 85% (76–91%), and negative predictive value of 77% (67–85%). For patients with AC stroke, the sensitivity of a baseline NIHSS score ≤5 to predict a favorable outcome was 65% (95% CI 55–73%), and the specificity was 89% (81–95%). For patients with PC stroke, the specificity of a baseline NIHSS ≤8 to predict a favorable outcome was 46% (95% CI 27–67%), and the sensitivity was 93% (85–98%).

The analysis was also performed for predicting the outcome, corresponding to mRS of 0 to 1. The AUC of the ROC curve in patients with PC stroke was 0.896 (95% CI 0.834–0.958) and that in patients with AC stroke was 0.801 (95% CI 0.741–0.861). For patients with PC stroke, the optimal cutoff score of the baseline NIHSS was ≤5 with a sensitivity of 93% (95% CI 84–98%) and specificity of 69% (53–82%). For patients with AC stroke, the optimal cutoff score was ≤8 with a sensitivity of 85% (95% CI 75–92%) and specificity of 66% (95% CI 58–74%).

DISCUSSION In this study, we assessed the relationship between baseline neurologic severities evaluated using the NIHSS and the chronic outcome of patients with ischemic strokes involving different arterial territories, determined primarily

Table 2 Baseline NIH Stroke Scale subscores

	Anterior circulation (n = 198)					Posterior circulation (n = 96)					
Items	0	1	2	3	4	0	1	2	3	4	p Value
#1A Level of consciousness	115	68	15			78	16	1	1		<0.001
#1B Questions	126	20	52			86	5	5			<0.001
#1C Commands	155	16	27			93	1	2			<0.001
#2 Gaze	141	46	11			85	9	2			0.001
#3 Visual fields	177	17	4			78	11	5	2		0.043*
#4 Facial palsy	61	87	50			56	34	5	1		<0.001
#5 Motor arm											
a. Left	124	28	12	12	22	73	10	9	3	1	0.010
b. Right	110	40	16	16	16	67	17	7	3	2	0.008
#6 Motor leg											
a. Left	120	30	18	16	14	71	12	10	1	2	0.011
b. Right	110	33	24	12	19	70	11	11	1	3	0.002
#7 Ataxia	186	8	4			67	19	10			<0.001*
#8 Sensory	98	79	20	1		55	37	4			0.111
#9 Language	137	18	19	24		88	5	1	2		<0.001
#10 Dysarthria	70	99	29			41	45	10			0.168
#11 Extinction/inattention	140	31	27			92	4				<0.001

Number indicates patient number. Eleven patients with anterior circulation stroke and five patients with posterior circulation stroke were excluded because of missing data.
*The posterior circulation group's scores are higher than those of the anterior circulation group.

using diffusion-weighted MRI. The major findings of this study were that optimal cutoff NIHSS scores to predict a favorable chronic outcome differed in patients with AC and PC stroke, and patients with PC stroke had a high probability of an unfavorable outcome at 3 months with relatively low NIHSS scores.

Although the NIHSS is the most widely used scoring system in patients with stroke and is highly predictive of chronic outcome, it has a potential weakness with respect to uneven scoring of lesion-specific neurologic deficits. For example, a right hemispheric stroke receives a low NIHSS score compared with the same-sized left hemispheric stroke, partly because the NIHSS awards seven points for tests directly related to language function and only two points for neglect.[11,19] There appear to be similar concerns when the NIHSS is used to compare patients with AC and PC stroke. The scale is highly weighted toward AC deficits, including cortical signs and motor function, while PC deficits, including cranial nerve signs and ataxia, receive fewer points[4,14]; ataxia is frequently excluded from scoring due to the coexistence of motor deficits. Thus, NIHSS may not appropriately evaluate the spectrum of PC-related signs. This weakness seems to be an important cause of the difference between AC and PC stroke in the NIHSS cutoff scores for predicting chronic outcome. Even the mRS has a weakness in that it is highly focused on the ability to walk and perform the usual activities of daily living.[4,20]

At present, thrombolysis using IV recombinant tissue plasminogen activator (rt-PA) is the most effective therapy for acute ischemic stroke. In several key thrombolysis studies, the NIHSS has always been used to assess baseline patient severity and sometimes to assess final outcome.[5,21-23] In a series of infarcts presenting within 3 hours, the presence of mild symptoms was the leading reason why patients did not receive thrombolysis.[24] Some trials excluded patients with baseline NIHSS scores of ≤4, as they were considered to have had a mild stroke[22,23]; clinically, such patients may be considered ineligible for IV rt-PA. However, the NIHSS cutoff score predicting a favorable outcome for patients with PC stroke (≤5) is close to 4; thus, one should not simply refrain from thrombolysis in patients with PC stroke with a relatively low NIHSS score, but one should consider thrombolysis if the PC-specific deficits that were underestimated by NIHSS warrant rt-PA. A recent study warned that a substantial